ELSEVIER

Coordination Chemistry Reviews
215 (2001) 1–37

COORDINATION CHEMISTRY REVIEWS

www.elsevier.com/locate/ccr

The chemistry of Group 13/15 compounds (III–V compounds) with the higher homologues of Group 15, Sb and Bi

Stephan Schulz *

Institut für Anorganische Chemie der Universität Bonn, Gerhard-Domagk-Str.1, D-53121 Bonn, Germany

Received 7 March 2000; accepted 2 May 2000

Contents

* Tel.: +49-228-735326; fax: +49-228-735327.
E-mail address: sschulz@uni-bonn.de (S. Schulz).

PII: S0010-8545(00)00401-X

Abstract

$Sb(SiMe_3)_3$ reacts with R_3M (R = Alkyl, M = Al, Ga, In) to form simple Lewis acid–base adducts $R_3M \leftarrow SbR'_3$. Reactions with R_2MCl (R = Me, Et, *t*-Bu) do not give uniform reaction products. Ga and In derivatives react under dehalosilylation to give heterocyclic compounds of the type $[R_2MSb(SiMe_3)_2]_x$ ($x = 2, 3$). In contrast, Me_2AlCl leads to the formation of the six-membered heterocycle $[Me(Cl)AlSb(SiMe_3)_2]_3$. Sterically more demanding diorgano aluminum halides Et_2AlCl and $t\text{-}Bu_2AlCl$ form simple adducts $R_2AlCl \leftarrow Sb(SiMe_3)_3$ (R = Et, *t*-Bu). Heterocycles of the type $[R_2AlSbR'_2]_x$ ($x = 2, 3$) are obtained by dehydrosilylation reactions between dialkyl aluminum hydrides R_2AlH (R = Me, Et, *i*-Bu) and $R'_2SbSiMe_3$ (R′ = $SiMe_3$, *t*-Bu). This reaction pathway also leads to the first synthesis of an organometallic bismuthide of Group 13 elements, Al, Ga and In. $[Me_2AlBi(SiMe_3)_2]_3$ is formed by reaction of Me_2AlH with $Bi(SiMe_3)_3$ and its structure, as determined by X-ray crystallography, clearly reveals the formation of a six-membered heterocycle in the solid state. Monomeric aluminum stibides $R_2AlSbR'_2 \leftarrow$ dimethylaminopyridine (dmap) are synthesized by reaction of the corresponding heterocycles $[R_2AlSbR'_2]_x$ with dmap. Pyrolyses of Ga and In adducts, as well as Ga and In heterocycles, yield nanocrystalline GaSb and InSb through a β-hydride elimination pathway. Detailed metalorganic chemical vapor deposition investigations also demonstrate the potential of Al–Sb heterocycles $[R_2AlSb(SiMe_3)_2]_2$ (R = Et, *i*-Bu) to produce AlSb thin films. In addition, GaSb can be prepared in solution by a dehalosilylation reaction between $GaCl_3$ and $Sb(SiMe_3)_3$. Depending on the solvent and its boiling point, nanoscale GaSb crystallites are obtained. Both the particle size and the composition can be controlled by the solvent.

Keywords: Antimony; Bismuth; Synthesis; Trialkyl compounds

1. Introduction

Within the last 30 years, several research groups have focused on the preparation of Group 13–15 compounds. There are two main reasons for these very intense studies.

1. The compounds are of fundamental interest owing to their bonding properties. Tremendous efforts were undertaken concerning the synthesis of monomeric compounds of the type $R_2MER'_2$ and the determination of their solid-state structures in an attempt to obtain further insight into the nature of the M–E bond. Theoretical investigations to determine whether or not the M–E bond has a partial double bond character were also performed [1]. Monomeric compounds RMER′ (M = Al, Ga, In, Tl; E = N, P, As, Sb, Bi) are still unknown, in contrast to the well-known boron compounds $R_2B{=}ER_2$, which contain σ- and π-bonding parts (E = N, P) [2]. However, the dimeric and trimeric forms $[RMER']_2$ and $[RMER']_3$ (M = Al, Ga; E = N, P, As), which are now prevalent in the literature, are also of theoretical interest owing to their number of π-electrons (quasi-aromaticity, anti-aromaticity) [3].

2. Most binary III–V materials (ME) are semiconductors with narrow direct band gaps between 0.17 (InSb) and 6.20 eV (AlN). Their interesting physical properties render them very promising candidates for several applications in opto- and micro-electronics devices. Several synthetic routes for their are preparation known, e.g. molecular beam epitaxy (MBE) or liquid phase epitaxy (LPE) processes. Since the pioneering work of Manasevit in 1968 [4], who first described clearly the metalorganic chemical vapor deposition (MOCVD) process using two starting compounds (Et_3Ga and AsH_3) for the synthesis of GaAs layers, several research groups have demonstrated this technology to be generally useful for the synthesis of thin films of metals, semiconducting or superconducting materials. In an extension of these studies, the potential of compounds containing both elements connected by a chemical bond (so-called single-source precursors) for the deposition of thin films of the corresponding material by MOCVD technology was demonstrated. Therefore, chemists became very interested in the synthesis of those precursors and developed different general pathways for their synthesis.

Numerous compounds $[R_2MER'_2]_x$ and $[RMER']_x$, most of them containing the lighter elements of Group 15 (E = N, P, As), have been synthesized and structurally characterized [5]. This is mainly due to the fact that several synthetic pathways for their synthesis have been known for many years. Powerful and generally useful synthetic routes are alkane elimination (Eq. (1)) and salt elimination (Eq. (2)) reactions. In addition, dehalosilylation reactions became popular (Eq. (3)), in particular for the synthesis of Ga–As and In–As compounds. The use of the very toxic arsanes R_2AsH, $RAsH_2$ and AsH_3 is avoided and the workup is very easy [6].

$$MR_3 + EH_3 \longrightarrow R_3M \leftarrow EH_3 \longrightarrow 1/x[R_2MEH_2]_x + RH \longrightarrow 1/x[RMEH]_x + RH$$

$x \geq 2$

M = Al, Ga, In; E = N, P, As; R, R′ = organic ligand (1)

$$R_2MX + M'ER'_2 \longrightarrow 1/x[R_2MER'_2]_x + M'X \quad x \geq 2$$

M = Al, Ga, In; X = halogen; M′ = Li, Na, K; E = N, P, As; R, R′ = organic ligand (2)

$$R_2MX + E(SiMe_3)_3 \longrightarrow 1/x[R_2ME(SiMe_3)_2]_x + Me_3SiX \quad x \geq 2$$

M = Al, Ga, In; X = halogen; E = P, As; R = X, organic ligand (3)

On the other hand, investigations concerning the synthesis of Group 13/15 precursors with the higher homologues of Group 15, Sb and Bi, have been very rare. In the early 1950s, Coates investigated the adduct formation between gallium trialkyls R_3Ga and trialkyl pnicogenides R_3E. Reactions of Me_3Ga with Me_3N, Me_3P, Me_3As and Me_3Sb led to the formation of the corresponding Lewis acid-base adducts, whereas Me_3Bi did not react [7]. It was found that the adduct strength decreased from R_3N to R_3Sb. Krannich and coworkers investigated reactions between $Sb(NMe_2)_3$ and AlR_3, which form aminoalanes $(R_2AlNR'_2)_x$ and R_3Sb; adduct formation, as found in the analogous reaction with $As(NMe_2)_3$, was not observed [8].

Until 4 years ago, only a handful of organometallic Group 13 antimonides had been prepared and structurally characterized. Group 13 bismuthides were completely unknown. $(Cp^*Al)_3Sb_2$ (**1**), an unusual compound with two 'naked' Sb atoms bridged by three Cp*Al fragments, was synthesized by Roesky and coworkers, but its structure could not be investigated in detail [9]. Cowley and coworkers synthesized four compounds containing Ga–Sb and In–Sb σ-bonds. Reactions of t-Bu_2SbLi with Me_2GaCl and Me_2InCl gave the six-membered heterocycles $[Me_2GaSb(t\text{-}Bu)_2]_3$ (**2**) and $[Me_2InSb(t\text{-}Bu)_2]_3$ (**3**), whereas addition of t-$Bu_2SbSiMe_3$ to $GaCl_3$ and $InCl_3$ resulted in the formation of $[Cl_2GaSb(t\text{-}Bu)_2]_3$ (**4**) and $[t\text{-}Bu_2Sb(Cl)In\text{-}\mu\text{-}Sb(t\text{-}Bu)_2]_2$ (**5**) [10].

Since 1996, our group and that of Wells have investigated in detail the synthesis of Group 13 stibides. While the Wells group focused on the preparation of Ga and In derivatives, we concentrated on the synthesis of aluminum stibides. These studies have led to the synthesis of several new compounds, which are the object of this review. More than 20 compounds have been structurally characterized to give a deeper insight into the structural features of these compounds. They can be divided into two general classes:

1. simple Lewis acid–base adducts $R_3M \leftarrow SbR'_3$ with dative M–Sb bonds;
2. compounds with a σ-bond between the Group 13 element and Sb, mainly in the form of four- and six-membered heterocycles $[R_2MSbR'_2]_x$. Very recently, monomeric Lewis base-stabilized compounds $R_2AlSbR'_2 \leftarrow$ dmap (dmap = dimethylaminopyridine) were synthesized in our group by ring cleavage reactions.

2. Lewis acid–base adducts $R_3M \leftarrow SbR'_3$ (M = Al, Ga, In)

2.1. Syntheses and solid-state structures

The tendency of Group 13 trialkyls to form adducts of the type $R_3M \leftarrow D$ (D = Lewis base) is a general aspect of their chemistry. Numerous adducts of Al, Ga and In trialkyls with amines, phosphines and arsines were synthesized and their structure determined by X-ray diffraction. This provided information about their bond strengths and the influence of steric and electronic factors [11]. In addition, several theoretical investigations were performed [12]. Very recently, the role of terminal atoms X in the donor–acceptor complexes $MX_3 \leftarrow D$ (M = Al, Ga, In; $X^- = Hal^-$; D = X^-, EX_3, EH_3; E = N, P, As) was investigated [13]. The bond strength of Group 13/15 Lewis acid–base adducts decreases for a constant Group 13 trialkyl from N to Bi and for a constant Group 15 trialkyl from Al to In. Therefore, Al–N adducts are the strongest adducts and In–Bi adducts the weakest adducts. These findings are in agreement with the HSAB principle of hard/weak Lewis acids/bases [14]. The Lewis acidity of Group 13 trialkyls, as indicated from dissociation enthalpies of $R_3M \leftarrow NMe_3$ adducts, takes the following order: $R_3B < R_3Al > R_3Ga > R_3In > R_3Tl$. The Lewis basicity of Group 15 trialkyls decreases in the following order: $R_3N > R_3P > R_3As > R_3Sb > R_3Bi$ [15]. Table 1 gives the dissociation enthalpies of various adducts.

The greatest number of structurally characterized adducts contain Al–N dative bonds. Within the last few years, these compounds, in particular AlH_3 adducts [16], have experienced a renaissance owing to their interesting bonding properties, as well as to their potential application to produce binary nitride materials MN. In contrast, reports on Group 13/15 Lewis acid–base adducts with the higher homologue of Group 15, Sb, are rare [17]. In 1996, Wells and coworkers began to synthesize adducts of the type $R_3M \leftarrow Sb(SiMe_3)_3$ (M = B, Ga, In) by adding boron trihalides [18] and gallium [19] and indium trialkyls [19a,20] to solutions of $Sb(SiMe_3)_3$ in pentane. We started our studies at the same time and reacted gallium trialkyls R_3Ga with both $Sb(SiMe_3)_3$ [21] and antimony trialkyls SbR'_3 [22]. In addition, the adduct formation of $Sb(SiMe_3)_3$ and SbR'_3 with aluminum trialkyls R_3Al and dialkyl aluminum chlorides R_2AlCl was investigated [23] (Scheme 1).

Up to now, more than 30 adducts have been synthesized and 12 of them structurally characterized. Table 2 gives an overview of the structurally characterized adducts, as well as the observed M–Sb bond lengths and X–Sb–X (X = C, Si) and C–M–C bond angles. Figs. 1–4 show the solid-state structures of four representative adducts.

Table 1
Dissociation enthalpies ΔH° of $R_3Al \leftarrow ER_3$ (E = N, P) 12b

Donor	Acceptor	ΔH° (kJ mol^{-1})	State of aggregation
H_3N	$AlMe_3$	27.6 ± 0.3	solution
Me_3N	$AlMe_3$	30.0 ± 0.2	solution
Et_3N	$AlMe_3$	26.5 ± 0.2	solution
Et_3P	$AlMe_3$	22.1 ± 0.3	solution
Ph_3P	$AlMe_3$	17.6 ± 0.2	solution
H_3N	$AlCl_3$	41	gas
Me_3N	$AlCl_3$	48 ± 2	solution
H_3N	$AlBr_3$	41.0	gas
Et_3N	$AlBr_3$	44.8	solution
Bu_3P	$AlBr_3$	47.5	solution
Ph_3P	$AlBr_3$	34.9	solution

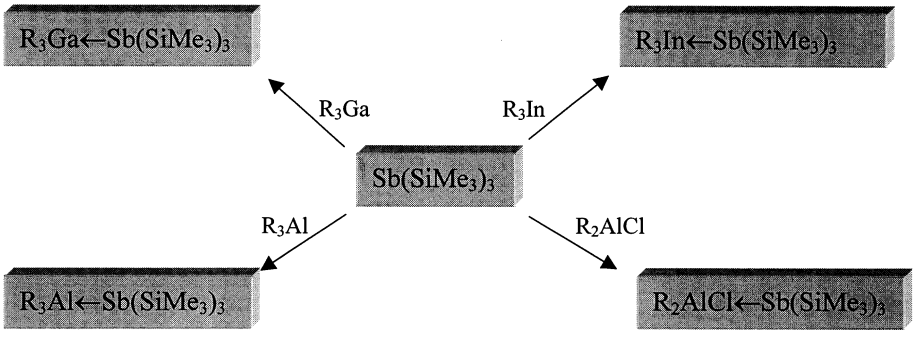

Scheme 1. Adduct formation reactions of $Sb(SiMe_3)_3$.

Table 2
M–Sb bond lengths, X–Sb–X (X = C, Si) and C–M–C bond angles of structurally characterized adducts

Adduct	M–Sb (pm)	X–Sb–X (°)	C–M–C (°)
$R_3Al \leftarrow Sb(SiMe_3)_3$			
R = Et (**6**) [23a]	284.10(5)	102.38(2)–104.74(2)	115.48(8)–115.99(8)
R = *i*-Bu (**7**) [24]	284.79(5)	102.60(2)–106.56(2)	115.73(6)–117.43(7)
$R_2AlCl \leftarrow Sb(SiMe_3)_3$			
R = *t*-Bu (**8**) [a] [23a]	282.11(6); 279.84(6)	102.87(2)–106.27(2); 100.25(2)–106.34(2)	119.96(9); 119.28(8)
$R_3Al \leftarrow SbR'_3$			
R = Me, R′ = *t*-Bu (**9**) [23b]	283.44(10)	106.20(14)–106.65(15)	115.4(6)–116.1(4)
R = Et, R′ = *t*-Bu (**10**) [23b]	287.30(9)	105.68(12)–106.15(12)	114.07(15)–115.35(15)
R = *t*-Bu, R′ = *i*-Pr (**11**) [23b]	292.67(4)	98.85(6)–101.43(6)	115.22(6)–115.83(6)
R = *t*-Bu, R′ = Et (**12**) [23b]	284.47(7)	97.91(11)–98.30(11)	115.89(11)–116.46(11)
$R_3Ga \leftarrow Sb(SiMe_3)_3$			
R = Et (**13**) [19a]	284.6(5)	102.2(3)–104.3(3)	114.5(12)–117.6(11)
R = *t*-Bu (**14**) [19b]	302.7(2)	100.65(8)–100.75(13)	116.7(3)–117.5(5)
$R_3Ga \leftarrow SbR'_3$			
R = *t*-Bu_3; R′ = Et (**15**) [22]	284.79(5)	97.32(18)–97.91(19)	115.88(17)–116.71(17)
R = *t*-Bu_3; R′ = *i*-Pr (**16**) [22]	296.18(2)	98.29(6)–101,33(7)	115.70(7)–116.20(7)
$R_3In \leftarrow Sb(SiMe_3)_3$			
R = Me_3SiCH_2 (**17**) [19a]	300.78(6)	104.29(6)	117.71(9)

[a] Two molecules within the asymmetric unit.

The solid-state structures of seven Al–Sb, four Ga–Sb and one In–Sb adducts have been determined. In each adduct, the ligands bound to the metal centers adopt a staggered conformation in relation to one other. The M–Sb bond lengths (M = Al, Ga) differ significantly due to the steric demand of the substituents. The Al–Sb distances observed for the adducts differ by only 13 pm (279.84(6) pm (**8**)–292.67(4) pm (**11**)) and those of the Ga–Sb adducts differ by 18 pm (284.6(5) pm (**13**)–302.7(2) pm (**14**)).

The Al–Sb bond length depends on the steric bulk of the ligands rather than on the ligand electronic properties. This is clearly revealed by comparison of the adducts **9** and **10** or **11** and **12**, where either the Sb fragment (Lewis base) or the Al fragment (Lewis acid) remains constant. The bond lengths increase in proportion to the steric demand of the ligands from 283.44(10) (**9**) to 287.30(9) pm (**10**) and from 284.47(7) pm (**12**) to 292.67(4) pm (**11**), respectively. The increase from **9** to **10** is easily explained by the decreased Lewis acidity of Et_3Al compared with Me_3Al, as well as by its increased steric demand due to the bulkier Et groups. Comparable

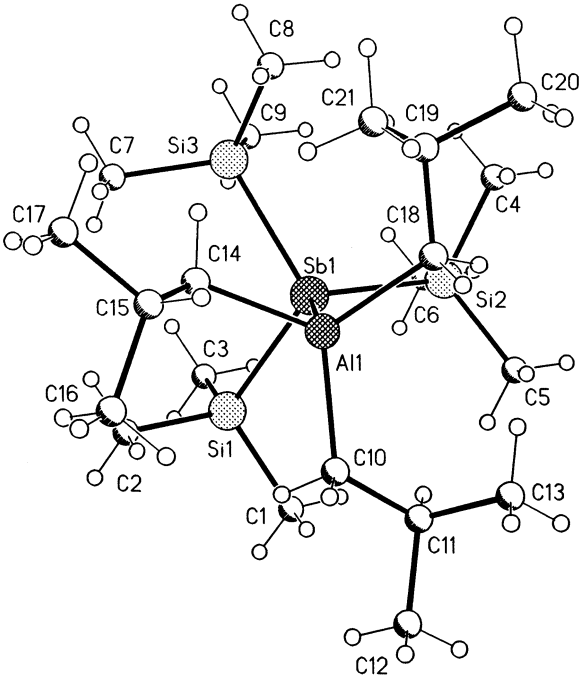

Fig. 1. Solid-state structure of **7**.

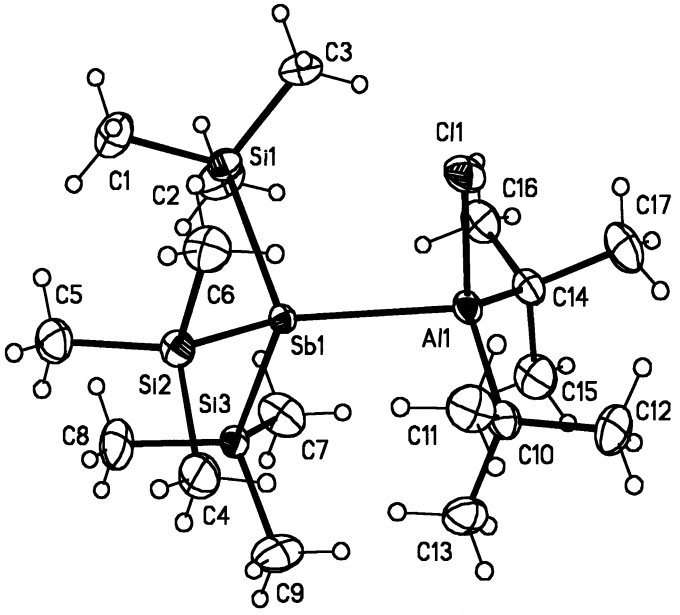

Fig. 2. Solid-state structure of **8**.

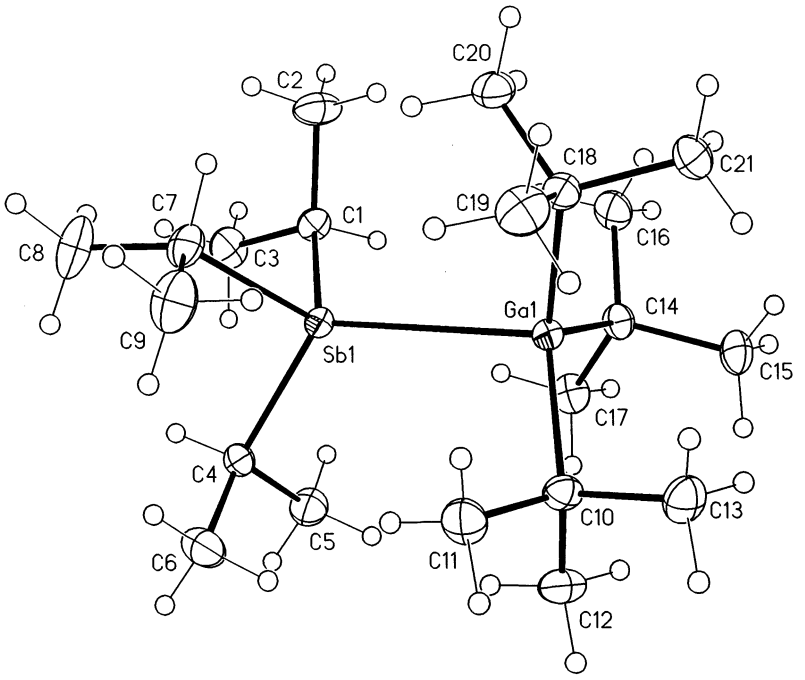

Fig. 3. Solid-state structure of **16**.

bond length differences are observed for $H_3Al \leftarrow NMe_3$ and $Me_3Al \leftarrow NMe_3$ (206 to 210 pm) [12b]. In contrast, the increase from **12** to **11** is caused only by the stronger steric repulsion between the ligands, because *i*-Pr_3Sb (**11**) is formally the stronger base compared with Et_3Sb (**12**). However, the $Sb(SiMe_3)_3$ adducts **6** and **7** [24] do not show this tendency. The Al–Sb distances found are almost equal (284.10(5) (**6**) and 284.79(5) pm (**7**)) despite the greater steric demand of three *i*-Bu groups compared with three Et groups (effective steric parameters: Et: 0.56; *i*-Bu: 0.98) [25]. The shortest Al–Sb distance is found in **8** (279.84(6) and 282.11(6) pm). *t*-Bu_2AlCl is the strongest Lewis acid within this group due to the electron density withdrawing effect of the chlorine atom, leading to a stronger adduct formation. In this case, the acidity (electronic aspect) dominates the ligand repulsion (steric aspect). Again, Al–N adducts show the same tendency (e.g. Me_3N–$AlMe_3$: 210 pm; Me_3N–$AlCl_3$: 196 pm).

An almost analogous influence of the ligand size is observed for the Ga–Sb bond distances. However, the effect is greater for the Ga–Sb than for the Al–Sb adducts. The bond length observed in *t*-$Bu_3Ga \leftarrow SbEt_3$ (284.6(5) pm) is almost the same as that in *t*-$Bu_3Al \leftarrow SbEt_3$ (284.10(5) pm), which is to be expected since the covalent radii of Al and Ga are equal (covalent radii: Al = Ga: 126 pm) [26]. In contrast, the distances for the $Sb(i\text{-}Pr)_3$ adducts (**11**, **16**) differ significantly by almost 4 pm

(t-$Bu_3Al \leftarrow Sbi$-Pr_3: 292.67(4) pm (**11**), t-$Bu_3Ga \leftarrow Sbi$-Pr_3: 296.18(2) pm (**16**)). This may be explained by the stronger Lewis acidic character of aluminum trialkyls compared with gallium trialkyls (electronegativity X: Ga = 1.81 > Al = 1.61) [27]. The M–E bond lengths in $Et_3Al \leftarrow Sb(SiMe_3)_3$ (284.10(5) pm) and $Et_3Ga \leftarrow Sb(SiMe_3)_3$ (284.6(5) pm) again are almost identical. The distance of 284 pm seems to be the shortest value that trialkyl aluminum and trialkyl gallium compounds as Lewis acids can reach in SbR'_3 adducts (R′ = alkyl, $SiMe_3$). Shorter M–Sb distances would lead to an increased steric repulsion between the ligands, which can be overcome only by a stronger Lewis acid, e.g. through substitution of one alkyl group by a chlorine atom. As expected, the longest Ga–Sb bond length is observed in the sterically overcrowded adduct t-$Bu_3Ga \leftarrow Sb(SiMe_3)_3$ **14** (302.7(2) pm).

Up to now, the only structurally characterized In–Sb adduct is $(Me_3SiCH_2)_3In \leftarrow Sb(SiMe_3)_3$ (**17**) [19a]. The In–Sb bond distance was determined to be 300.78(6) pm. However, this distance is supposedly at the lower end of the In–Sb dative bond range, because the covalent radius of In (r_{cov} = 143 pm) is about 17 pm larger than those of Al and Ga (r_{cov} = 126 pm). Bearing in mind that the steric pressure of the

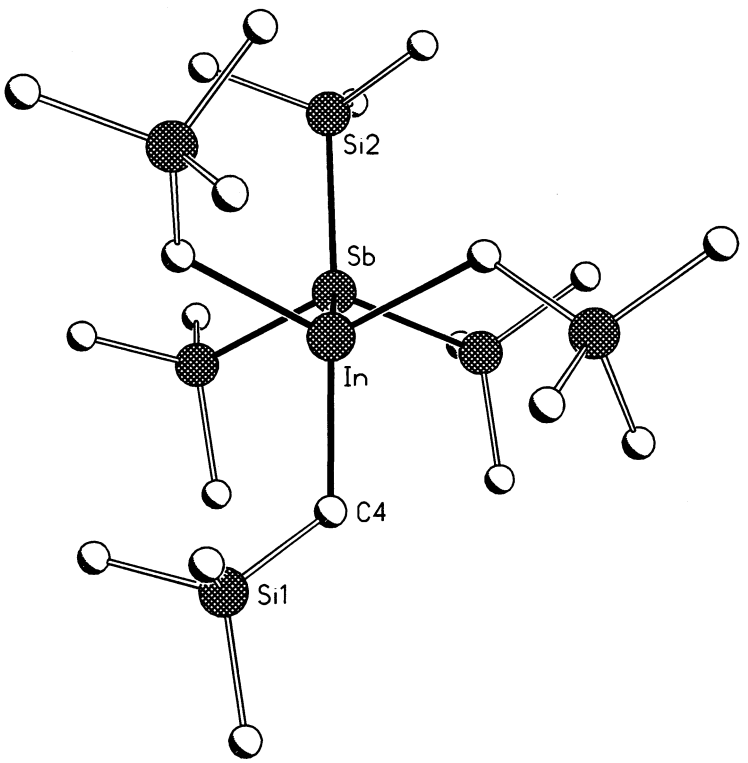

Fig. 4. Solid-state structure of **17**.

Table 3
Selected ^{1}H- and ^{13}C-NMR shifts and Δ(H) and Δ(C) values and internal shifts Δ_{H-H} and Δ_{C-C} of Al trialkyls and the adducts in C_6D_6

Compound	δ ^{1}H[a]	δ ^{13}C[b]	Δ(H)[c]	Δ(C)[d]
Me_3Al	−0.36	−6.79		
$Me_3Al \leftarrow SbEt_3$	−0.32	−6.38	0.04	0.41
$Me_3Al \leftarrow Sb(n\text{-}Pr)_3$	−0.33	−6.67	0.03	0.12
$Me_3Al \leftarrow Sb(i\text{-}Pr)_3$	−0.28	−5.39	0.08	1.40
$Me_3Al \leftarrow Sb(sec\text{-}Bu)_3$	−0.32	−6.38	0.04	0.41
$Me_3Al \leftarrow Sb(t\text{-}Bu)_3$	−0.21	−5.02	0.15	1.77
Et_3Al	0.31	0.87		
$Et_3Al \leftarrow SbEt_3$	0.35	2.40	0.04	1.53
$Et_3Al \leftarrow Sb(n\text{-}Pr)_3$	0.33	1.88	0.02	0.99
$Et_3Al \leftarrow Sb(i\text{-}Pr)_3$	0.37	2.62	0.06	1.75
$Et_3Al \leftarrow Sb(sec\text{-}Bu)_3$	0.37	2.54	0.06	1.67
$Et_3Al \leftarrow Sb(t\text{-}Bu)_3$	0.42	3.70	0.11	2.83
$t\text{-}Bu_3Al$	1.08	21.09		
$t\text{-}Bu_3Al \leftarrow SbEt_3$	1.27	19.10	0.19	−2.01
$t\text{-}Bu_3Al \leftarrow Sb(n\text{-}Pr)_3$	1.30	19.10	0.22	−2.01
$t\text{-}Bu_3Al \leftarrow Sb(i\text{-}Pr)_3$	1.26	19.58	0.18	−1.51
$t\text{-}Bu_3Al \leftarrow Sb(sec\text{-}Bu)_3$	1.21	20.27	0.13	−0.82
$t\text{-}Bu_3Al \leftarrow Sb(t\text{-}Bu)_3$	1.09	21.24	0.01	0.15

[a] Me_3Al and Et_3Al: δ ^{1}H (α-H); $t\text{-}Bu_3Al$: δ ^{1}H (β-H).
[b] Me_3Al and Et_3Al: δ ^{13}C (α-C); $t\text{-}Bu_3Al$: δ ^{13}C (α-C).
[c] Me_3Al and Et_3Al: $\Delta(H) = \delta(\alpha\text{-}H)_{adduct} - \delta(\alpha\text{-}H)_{trialkylalane}$; $t\text{-}Bu_3Al$: $\Delta(H) = \delta(\beta\text{-}H)_{adduct} - \delta(\beta\text{-}H)_{trialkylalane}$.
[d] Me_3Al and Et_3Al: $\Delta(C) = \delta(\alpha\text{-}C)_{adduct} - \delta(\alpha\text{-}C)_{trialkylalane}$; $t\text{-}Bu_3Al$: $\Delta(C) = \delta(\alpha\text{-}C)_{adduct} - \delta(\alpha\text{-}C)_{trialkylalane}$.

ligands is not as effective for the larger In atom as it is for the smaller Al and Ga atom, the In–Sb dative bond length range is estimated to be between 300 and 315 pm. Further investigations have to be performed to obtain deeper insights into the structural features of those adducts.

2.2. Multinuclear NMR investigations

In an attempt to determine the M–Sb bond strength in solution by NMR experiments, a series of completely alkylated Al–Sb and Ga–Sb adducts was studied by ^{1}H and ^{13}C spectroscopy. Table 3 gives an overview of the chemical shifts δ and the differences Δ in the chemical shifts compared with the pure aluminum trialkyl obtained for the Al–Sb adducts; those for the Ga–Sb adducts are summarized in Table 4.

In each adduct the resonances of the organic ligands bound to the Group 13 element are shifted to lower field compared with the pure trialkyl, whereas those of the organic ligands bound to Sb are shifted to higher field. Comparable results were obtained in adducts of the type $Me_3Al \leftarrow PR_3$ [11a], $R_3Ga \leftarrow PR'_3$ (R = Me, Et)

Table 4
Selected ^{1}H- and ^{13}C-NMR shifts, Δ(H), Δ(C) values and internal shifts Δ_{H-H} and Δ_{C-C} of the Ga trialkyls and the adducts in C_6D_6

Compound	δ ^{1}H[a]	δ ^{13}C[b]	Δ(H)[c]	Δ(C)[d]
n-Bu_3Ga	0.61	19.3		
n-$Bu_3Ga \leftarrow SbEt_3$	0.73	16.1	0.12	−3.2
n-$Bu_3Ga \leftarrow Sb(n\text{-}Pr)_3$	0.66	16.9	0.05	−2.4
n-$Bu_3Ga \leftarrow Sb(i\text{-}Pr)_3$	0.74	16.6	0.13	−2.7
n-$Bu_3Ga \leftarrow Sb(t\text{-}Bu)_3$	0.80	16.4	0.19	−2.9
t-Bu_3Ga	1.16	31.5		
t-$Bu_3Ga \leftarrow SbEt_3$	1.32	26.9	0.16	−4.6
t-$Bu_3Ga \leftarrow Sb(n\text{-}Pr)_3$	1.32	27.3	0.16	−4.2
t-$Bu_3Ga \leftarrow Sb(i\text{-}Pr)_3$	1.23	30.0	0.07	1.5
t-$Bu_3Ga \leftarrow Sb(t\text{-}Bu)_3$	1.16	31.5	0	0

[a] *n*-Bu_3Ga: δ ^{1}H (α-H); *t*-Bu_3Ga: δ ^{1}H (β-H).
[b] *n*-Bu_3Ga: δ ^{13}C (α-C); *t*-Bu_3Ga: δ ^{13}C (α-C).
[c] *n*-Bu_3Ga: $\Delta(H) = \delta(\alpha\text{-}H)_{adduct} - \delta(\alpha\text{-}H)_{trialkylgallane}$; *t*-$Bu_3Ga$: $\Delta(H) = \delta(\beta\text{-}H)_{adduct} - \delta(\beta\text{-}H)_{trialkylgallane}$.
[d] *n*-Bu_3Ga: $\Delta(C) = \delta(\alpha\text{-}C)_{adduct} - \delta(\alpha\text{-}C)_{trialkylgallane}$; *t*-$Bu_3Ga$: $\Delta(C) = \delta(\alpha\text{-}C)_{adduct} - \delta(\alpha\text{-}C)_{trialkylgallane}$.

[11b,28], and $Me_3In \leftarrow NR_3$ [29]. The Δ values observed for α-H and α-C resonances of Me_3Al, Et_3Al and *n*-Bu_3Ga adducts correlate with the basicity of the coordinated antimony trialkyls. The biggest low-field shifts of α-H and α-C resonances (and therefore biggest Δ(H) and Δ(C) values) of the Me, Et and *n*-Bu groups are observed in adducts with the electronically *strongest* Lewis base *t*-Bu_3Sb [30]. In contrast, ^{1}H-NMR spectra of the sterically hindered *t*-Bu_3Al and *t*-Bu_3Ga adducts show the biggest low-field shifts of β-H and α-C of the *t*-Bu group with the electronically *weakest* Lewis base Et_3Sb. The bulkier the groups at the Sb atom, the smaller is the low-field shift, indicating a weaker adduct in solution. This tendency reaches its maximum in adducts with *t*-Bu_3Sb, which show resonances at the same shift as the starting trialkyls, which is obviously a result of the complete dissociation of the adduct in solution [31]. These findings show clearly the contradictory influence of sterically bulky ligands: a bulkier ligand at the Sb atom leads not only to an increase in Lewis basicity but also to an increase in steric repulsion between acid and base. In the case of the sterically most demanding *t*-Bu_3Al/Ga–Sb(*t*-Bu)$_3$ adducts, the steric repulsion between the acid and the base fragment dominates the adduct strength, whereas in the case of the adducts with the sterically less bulkier Me_3Al, Et_3Al and *n*-Bu_3Ga acids the donor strength of the antimony base is decisive.

3. Heterocycles $[R_2MSbR'_2]_x$ (M = Al, Ga, In)

3.1. Syntheses and structures

Only a few examples of Group 13 stibides with σ-bonds between M and Sb were known until 1996. This is mainly due to the fact that synthetic pathways, which have been developed for the preparation of Group 13 amides, phosphides and arsenides, are not successful. Alkane elimination reactions, for example, do not work because the Sb–H Group is less protic than the N–H and P–H group (electronegativity *X*: N: 3.04; P: 2.19; As: 2.18; Sb: 2.05) [27]. In addition, the bond energies of Group 13/15 compounds decrease from N to Sb, as can be seen in Table 5. Therefore, the formation of heterocycles with the higher homologues of Group 15, in particular Bi, is less favored thermodynamically.

Five examples of Al, Ga and In stibides were known previous to the studies by Wells and coworkers and by ourselves. They were prepared by reactions of $[Cp^*Al]_4$ with $[t\text{-BuSb}]_4$ (**4**), of $t\text{-Bu}_2\text{SbLi}$ with Me_2GaCl and Me_2InCl (**5**) and of $t\text{-Bu}_2\text{SbSiMe}_3$ with $GaCl_3$ and $InCl_3$ (**6**)

$$3/4[Cp^*Al]_4 + 3/4[t\text{-BuSb}]_4 \xrightarrow[-\ t\text{-Bu}_3\text{Sb}]{} (Cp^*Al)_3Sb_2\ (\mathbf{1}) \quad (4)$$

$$3t\text{-Bu}_2\text{SbLi} + 3Me_2MCl \xrightarrow[-\ 3LiCl]{} [Me_2MSb(t\text{-Bu})_2]_3\ (M = Ga\ (\mathbf{2}),\ In\ (\mathbf{3})) \quad (5)$$

$$3t\text{-Bu}_2\text{SbSiMe}_3 + 3GaCl_3 \xrightarrow[-\ 3Me_3SiCl]{} [Cl_2GaSb(t\text{-Bu})_2]_3\ (\mathbf{4})$$

$$4t\text{-Bu}_2\text{SbSiMe}_3 + 2InCl_3 \xrightarrow[-\ 4Me_3SiCl]{} (t\text{-Bu}_2\text{Sb(Cl)In-}\mu\text{-Sb(t-Bu)}_2]_2\ (\mathbf{5}) \quad (6)$$

The structure of $(Cp^*Al)_3Sb_2$ (**1**; Fig. 5) was not described in detail due to some disorder problems, but its connectivity was determined without any doubts [9]. The same structural feature was found in $(i\text{-Pr}_2\text{NB})_3P_2$ [32].

The six-membered heterocycles $[Me_2GaSb(t\text{-Bu})_2]_3$ (**2**) [10b], $[Cl_2GaSb(t\text{-Bu})_2]_3$ (**3**) [10a] and $[Me_2InSb(t\text{-Bu})_2]_3$ (**4**; Fig. 6) [10b] adopt distorted twist-boat-type conformations, with average M–Sb bond lengths of 266.1 pm for **3** and 285.5 pm for **4**. The distortion within the ring is reflected by the wide range of Ga–Sb and In–Sb bond lengths (in both about 8 pm) and the endocyclic ring angles (about 12°). In accordance with the VSEPR model, the angles at the Ga centers are greater than and those at the Sb atoms smaller than a tetrahedral arrangement. The planar, dimeric compound $[t\text{-Bu}_2\text{Sb(Cl)In-}\mu\text{-Sb}(t\text{-Bu})_2]_2$ (**5**; Fig. 7) [10c] shows two different

Table 5
Bond dissociation energies D°_{298} of heteronuclear M–E bonds in diatomic molecules [73]

M–E	D°_{298} (kJ mol^{-1})	M–E	D°_{298} (kJ mol^{-1})	M–E	D°_{298} (kJ mol^{-1})
Al–N	297 ± 96	Ga–N		In–N	
Al–P	216.7 ± 12.6	Ga–P	229.7 ± 12.6	In–P	197.9 ± 8.4
Al–As	202.9 ± 7.1	Ga–As	209.6 ± 1.2	In–As	201
Al–Sb	216.3 ± 5.9	Ga–Sb	192.0 ± 12.6	In–Sb	151.9 ± 10.5
Al–Bi	?	Ga–Bi	159 ± 17	In–Bi	153.6 ± 1.7

In–Sb bond distances, because this compound contains both a bridging and a terminal t-Bu_2Sb moiety bound to the In center. As expected, the In–Sb bond distance of the terminal, three-coordinated t-Bu_2Sb fragment (279.7 pm) is about 7 pm shorter than that of the bridging t-Bu_2Sb moiety (286.5 pm). In solution at ambient temperature, only one signal due to the t-Bu groups was observed, indicating a rapid interchange between the terminal and bridging moiety.

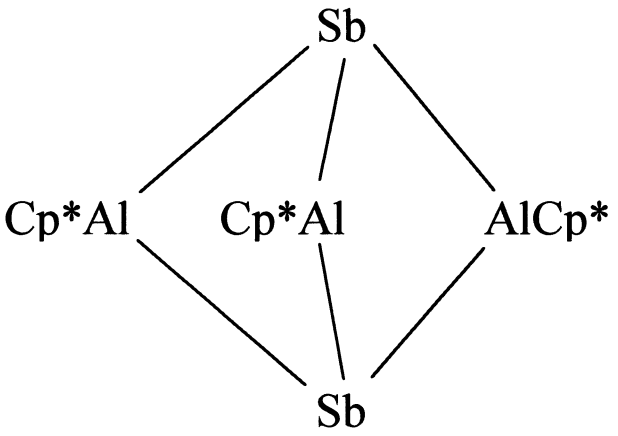

Fig. 5. Graphical representation of **1** showing its connectivity.

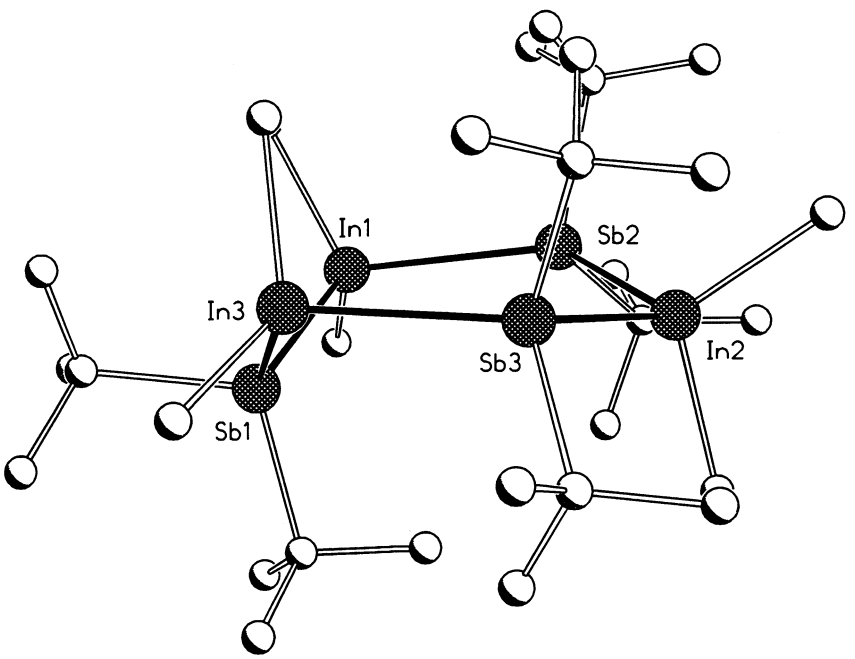

Fig. 6. Solid-state structure of **4**.

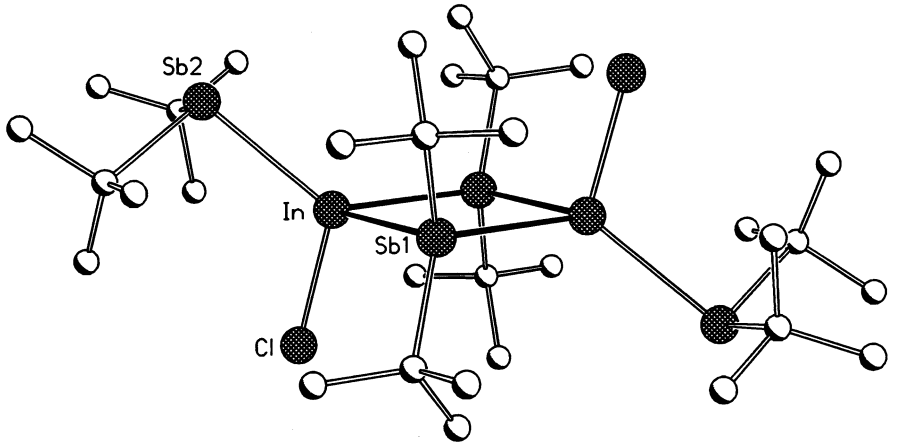

Fig. 7. Solid-state structure of **5**.

Since 1996, Wells and coworkers have prepared several Group 13 stibides in an analogous way to the syntheses of the corresponding phosphides and arsenides. Dehalosilylation reactions of diorganogallium or indium halides and $Sb(SiMe_3)_3$ gave four-membered heterocycles of the type $[R_2MSb(SiMe_3)_2]_2$.

$$2R_2MCl + 2Sb(SiMe_3)_3 \xrightarrow[-2Me_3SiCl]{} [R_2MSb(SiMe_3)_2]_2 \ (M = Ga, In) \quad (7)$$

$$2t\text{-}Bu_2GaCl + Sb(SiMe_3)_3 \xrightarrow[-Me_3SiCl]{} ((t\text{-}Bu_2)Ga)_2(Cl)Sb(SiMe_3)_2 \ (\mathbf{19}) \quad (8)$$

Five four-membered heterocycles were structurally characterized: $[t\text{-}Bu_2GaSb(SiMe_3)_2]_2$ (**18**; Fig. 8) [19b], $(t\text{-}Bu_2Ga)_2(Cl)Sb(SiMe_3)_2$ (**19**) [19b], $[Et_2GaSb(SiMe_3)_2]_2$ (**20**) [33], $[(Me_3SiCH_2)_2InSb(SiMe_3)_2]_2$ (**21**) [19a], and $[t\text{-}Bu_2InSb(SiMe_3)_2]_2$ (**22**) [20]. The six-membered ring $[Me_2GaSb(SiMe_3)_2]_3$ (**23**; Fig. 9) was synthesized in our group by reaction of Me_2GaCl with $Sb(SiMe_3)_3$ and its solid-state structure determined by X-ray crystallography [21]. Breunig et al. synthesized an InSb heterocycle by reaction of a distibane and an indium trialkyl under cleavage of the Sb–Sb bond [34].

$$Me_2SbSbMe_2 + In(CH_2SiMe_3)_3 \rightarrow [Me_2SbIn(CH_2SiMe_3)_2]_3 \ (\mathbf{24}) \quad (9)$$

The values of the M–Sb bond distances and M–Sb–M and Sb–M–Sb bond angles of **18**–**24** (M = Ga, In) are summarized in Table 6 [35].

The average Ga–Sb bond length of 269.1 pm found in $[Me_2GaSb(SiMe_3)_2]_3$ (**23**) is slightly elongated compared with those found in $[Cl_2GaSb(t\text{-}Bu)_2]_3$ (**2**) (266.1 pm). This is rather the result of electronic (stronger acidic character of the Ga atoms in **2** due to the electron-withdrawing ability of Cl atoms) rather than steric effects (effective steric parameters: Me, 0.52; Cl, 0.55) [25]. Six-membered rings (**2**, **23**) are generally formed with small ligands (Me, Cl) bound to Ga and In, except for **24**. In this compound the In atoms are substituted by the sterically more-demanding CH_2SiMe_3 groups. Sterically more-demanding ligands lead to the

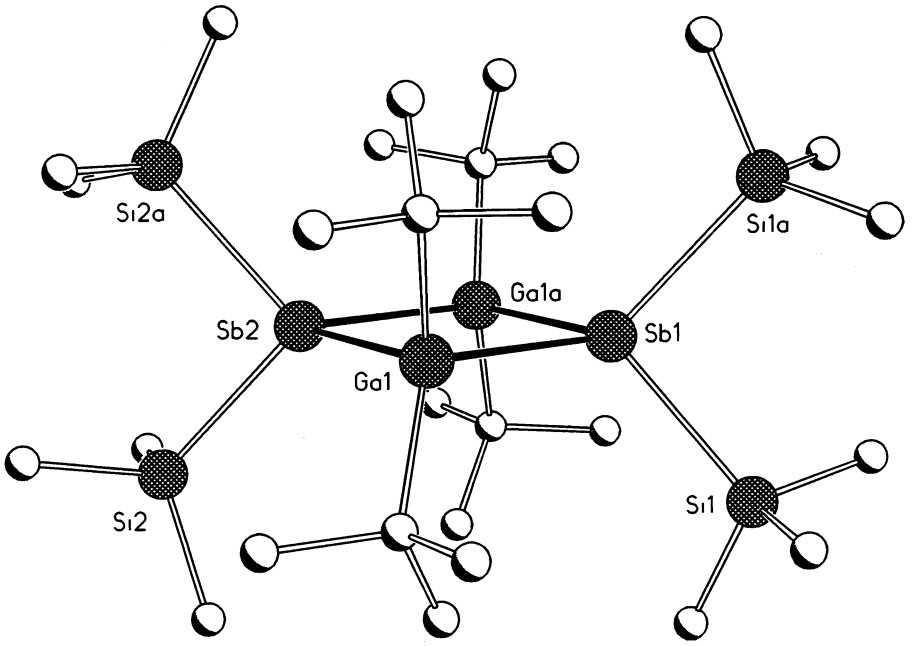

Fig. 8. Solid-state structure of **18**.

formation of four-membered heterocycles (**18**, **20**, **21**, **22**). Depending on the ligand size, both the M–Sb bond distances and the endocyclic bond angles of the dimeric compounds show significant differences. The average Ga–Sb distances range from 272.3 pm (**20**) to 276.7 pm (**18**) and the In–Sb distances from 288 pm (**21**) to 293.1 pm (**22**). This is significantly longer than the sum of the covalent radii (Ga–Sb: 264 pm; In–Sb: 281 pm) [26]. Compared with the six-membered rings, the M–Sb distances in four-membered rings are elongated, indicating the increased steric repulsion between the ligands.

If the reaction of t-Bu_2MCl and $Sb(SiMe_3)_3$ is performed in 2:1 stoichiometry, mixed bridge heterocycles are obtained. This is in contrast to the 1:2 reaction reported by Cowley and coworkers [10], which led to the heterocycle **5**. Although (t-$Bu_2In)_2Sb(SiMe_3)_2Cl$ is not stable in solution towards intermolecular dehalosilylation, and gives the dimer **22**, the Ga-containing ring (t-$Bu_2Ga)_2Sb(SiMe_3)_2Cl$ (**19**; Fig. 10) was isolated and structurally characterized. Compared with the dimer **18**, the Ga–Sb bond lengths (273.36(12) and 273.37(11) pm) are 3 pm shorter due to less steric repulsion and the electron-withdrawing influence of the Cl atom.

Our group was in particular interested in the synthesis of organometallic Al stibides, whose structures were unknown prior to our studies. In contrast to reactions with dialkyl gallium and indium chlorides, $Sb(SiMe_3)_3$ does not react with dialkyl aluminum chlorides R_2AlCl (R = Et, t-Bu) through dehalosilylation but through adduct formation ($R_2AlCl \leftarrow Sb(SiMe_3)_3$, see Section 2). This is mainly a result of the thermodynamically stronger Al–Cl bond compared with Ga–Cl and In–Cl bond (Table 7).

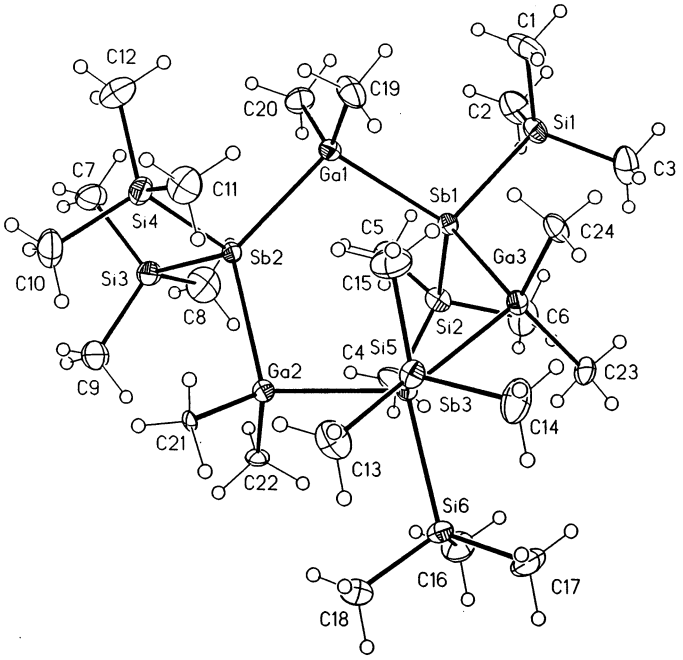

Fig. 9. Solid-state structure of **23**.

Table 6
M–Sb bond distances and M–Sb–M and Sb–M–Sb bond angles (M = Ga, In) of four-membered heterocycles

Compound	M–Sb (pm)	M–Sb–M (°)	Sb–M–Sb (°)
$[Me_2GaSb(SiMe_3)_2]_3$ (**23**) [21]	267.7(1)–271.4(1)	118.3(1)–127.6(1)	103.6(1)–107.3(1)
$[Et_2GaSb(SiMe_3)_2]_2$ (**20**) [33]	271.8(1), 272.9(1)	92.7(1)	87.3(1)
$[t\text{-}Bu_2GaSb(SiMe_3)_2]_2$ (**18**) [19b]	276.5(1), 276.8(1)	94.4(1), 94.5(1)	85.5(1)
$(t\text{-}Bu_2Ga)_2ClSb(SiMe_3)_2$ (**19**) [19b]	273.4(2)	85.7(1)	
$[t\text{-}Bu_2InSb(SiMe_3)_2]_2$ (**22**) [20]	292.73(2), 293.40(2)	94.83(1), 95.12(1)	85.03(1)
$[(Me_3SiCH_2)_2InSb(SiMe_3)_2]_2$ (**21**)[a] [19a]	288	95.2 (average)	84.8 (average)
$[Me_2SbIn(CH_2SiMe_3)_2]_3$ (**24**) [34]	285.19(6)–286.93(5)	129.2(1)–137.7(1)	92.4(1)–98.6(1)

[a] The poor quality of the crystals did not facilitate a complete data set collection.

However, the reaction of $Sb(SiMe_3)_3$ with Me_2AlCl proceeds through elimination of Me_4Si to the formation of the six-membered heterocycle $[Me(Cl)AlSb(SiMe_3)_2]_3$ (**25**) [36]. It is still unclear why the Al–Me bond is cleaved in this particular case but not in reactions with Me_3Al or $MeAlCl_2$. In these cases, even at higher temperatures no elimination reactions takes place.

$$3Me_2AlCl + 3Sb(SiMe_3)_3 \xrightarrow[-\,3Me_4Si]{} [Me(Cl)AlSb(SiMe_3)_2]_3\ (\mathbf{25}) \qquad (10)$$

In summary, the *dehalosilylation* reaction did not offer a general route for the preparation of Al–Sb heterocycles. Therefore, we searched for other possible pathways for their preparation, and realized that they can be generally synthesized by a *dehydrosilylation* reaction. Dialkyl aluminum hydrides R_2AlH react with $Sb(SiMe_3)_3$ or t-$Bu_2SbSiMe_3$ through elimination of Me_3SiH to give dimeric or trimeric heterocycles $[R_2AlSbR'_2]_x$ ($x = 2, 3$).

$$R_2AlH + Sb(SiMe_3)_3 \xrightarrow[-\,Me_3SiH]{} 1/x[R_2AlSb(SiMe_3)_2]_x \quad (11)$$

$$R_2AlH + t\text{-}Bu_2SbSiMe_3 \xrightarrow[-\,Me_3SiH]{} 1/x[R_2AlSb(t\text{-}Bu)_2]_x \quad (12)$$

Several compounds were synthesized, and five of them were characterized by X-ray analysis. They represent the first examples of organometallic Al–Sb ring compounds. The ring size depends on the steric bulk of the ligands bound to Al, as

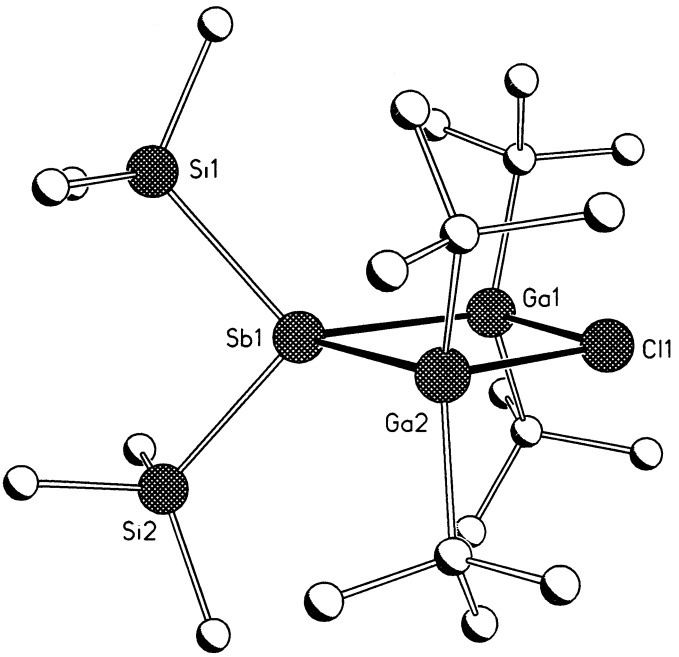

Fig. 10. Solid-state structure of **19**.

Table 7
Bond dissociation energies D°_{298}/kJ mol^{-1} of Al/Ga/In/Si–H/Cl/Sb bonds in diatomic molecules [73]

	Al	Ga	In	Si
H	284.9 ± 6.3	<274.1	243.1	≤ 299.2
Cl	511.3 ± 0.8	481 ± 13	439 ± 8	406
Sb	216.3 ± 5.9	192.0 ± 12.6	151.9 ± 10.5	?

Table 8
Al–Sb bond distances and Al–Sb–Al and Sb–Al–Sb bond angles of Al–Sb heterocycles

Compound	M–Sb (pm)	Al–Sb–Al (°)	Sb–Al–Sb (°)
$[Me_2AlSb(SiMe_3)_2]_3$ (**26**) [23a]	270.25(8)–273.62(8)	118.53(3)–128.24(2)	103.48(3)–106.52(3)
$[Et_2AlSb(SiMe_3)_2]_2$ (**28**) [39]	272.28(5), 272.92(5)	91.680(15)	88.320(15)
$[i\text{-}Bu_2AlSb(SiMe_3)_2]_2$ (**29**) [39]	274.29(5), 274.60(5)	93.660(15)	86.340(15)
$(Me_2Al)_3(Sb(t\text{-}Bu)_2)_2Sb(SiMe_3)_2$ (**30**) [37]	271.94(16)–278.03(16)	115.38(5)–128.37(5)	103.10(5)–106.89(5)
$[Me_2AlSb(t\text{-}Bu)_2]_3$ (**27**) [37]	271.88(10)–278.39(10)	115.28(3)–128.92(3)	102.80(3)–108.18(4)

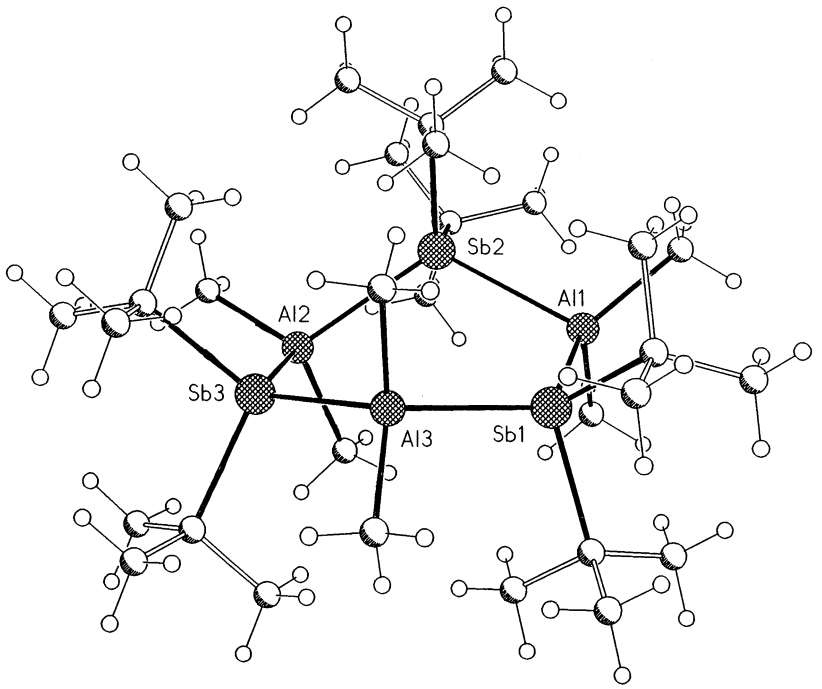

Fig. 11. Solid-state structure of **27**.

was found for the corresponding Ga stibides: small groups, like Me or Cl, favor the formation of six-membered rings $[Me_2AlSbR'_2]_3$, whereas Et and *i*-Bu groups lead to four-membered heterocycles $[R_2AlSbR'_2]_2$ (R = *t*-Bu, $SiMe_3$). Table 8 shows the Al–Sb bond distances and the endocyclic Al–Sb–Al and Sb–Al–Sb bond angles.

The six-membered heterocycles $[Me(Cl)AlSb(SiMe_3)_2]_3$ (**25**) [23a], $[Me_2AlSb(SiMe_3)_2]_3$ (**26**) [23a] and $[Me_2AlSb(t\text{-}Bu)_2]_3$ (**27**; Fig. 11) [37] are isostructural.

Their non-planar Al_3Sb_3 rings adopt distorted twist-boat conformations with both the Al and Sb atoms in distorted tetrahedral environments. The Al–Sb bond lengths observed for **27** (2.719(1)–2.784(1) Å) cover a wider range than those found in **26** (2.703(1)–2.737(1) Å). Despite the increased steric demand of Me_3Si compared with *t*-Bu groups (effective steric parameters: Me_3Si, 1.40; *t*-Bu, 1.24) [25], the ring is less strained owing to the replacement of a tertiary C atom (of *t*-Bu group) by a larger Si atom, as can also be seen by comparison of the bond angles (**26**: Si–Sb–Si = 100.67(3)–102.29(3) pm; **27**: C–Sb–C = 104.87(13)–106.02(14) pm). The average values of 2.75 Å (**27**) and 2.72 Å (**26**) are significantly elongated compared with the sum of the covalent radii of 264 pm for Al and Sb [26]. In agreement with the VSEPR model, the endocyclic Sb–Al–Sb bond angles are significantly smaller (**26**: 103.48(3)–106.52(3)°; **27**: 102.8(1)–108.2(1)°) and the Al–Sb–Al bond angles greater (**26**: 118.53(3)–128.24(2)°; **27**: 115.3(1)–128.9(1)°) than a tetrahedral arrangement. The same structural features were reported for other Al-pnictogen trimers [38].

In contrast to similar corresponding Ga–Sb and In–Sb heterocycles, the planar four-membered Al–Sb rings $[Et_2AlSb(SiMe_3)_2]_2$ (**28**; Fig. 12) and $[i\text{-}Bu_2AlSb(SiMe_3)_2]_2$ (**29**) [39] show Al–Sb bond lengths (**28**: 272.28(5)–272.92(5) pm; **29**: 274.29(5)–274.60(5) pm)) comparable to those found in six-membered rings. The bond angles (Al–Sb–Al: 91.68(2)° (**28**); 93.66(2) (**29**); Sb–Al–Sb: 88.32(2)° (**28**); 86.34(2) (**29**)) differ slightly and depend on the size of the organic ligands bound to Al. Sterically more-demanding *i*-Bu groups, evidenced by an increased C–Al–C

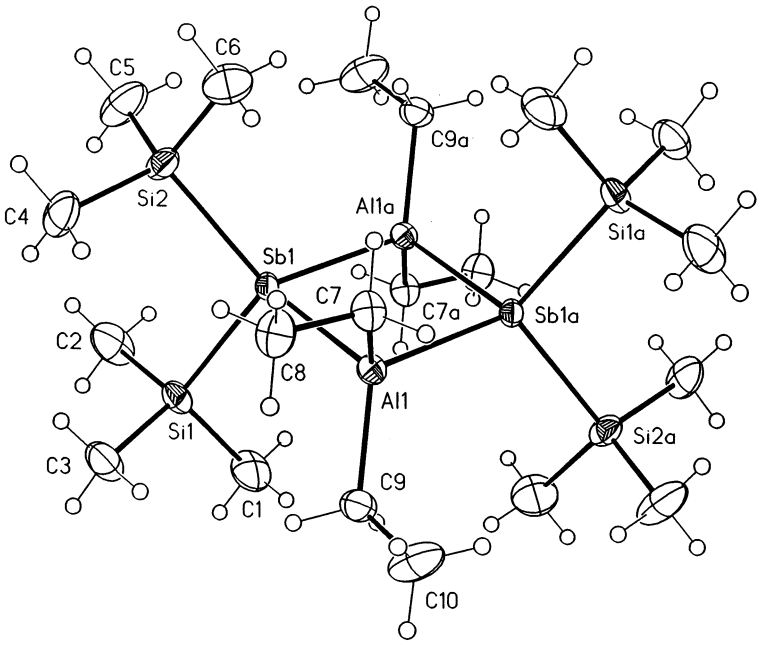

Fig. 12. Solid-state structure of **28**.

bond angle (121.2(1)° in **29** compared with 117.3(1)° in **28**), lead to smaller Sb–Al–Sb and bigger Al–Sb–Al angles. Analogous results were found in the related compounds $[R_2AlE(SiMe_3)_2]_2$ (R = Me, Et, *i*-Bu; E = P, As) [40], where the corresponding values show the same tendency, as can be seen in Table 9.

Analogously substituted Ga–Sb and Al–Sb rings show comparable bond distances. This is a surprise, because the Al fragment is the stronger Lewis acid. However, Ga and Al have the same covalent radii of 126 pm [41]. Here again, steric repulsion is dominating over electronic aspects in M–Sb heterocycles, as it is in M–Sb Lewis acid–base adducts (Scheme 2).

Table 9
Average bond lengths (pm) and angles (°) of four-membered heterocycles $[R_2AlE(SiMe_3)_2]_2$ (E = P, As, Sb)

$[R_2AlE(SiMe_3)_2]_2$	Al–E (pm)	Al–E–Al (°)	E–Al–E (°)	R–Al–R (°)	Si–E–Si (°)
$[Me_2AlP(SiMe_3)_2]_2$ [40a,b,c]	245.7	90.6	89.4	113.4	108.4
$[Et_2AlP(SiMe_3)_2]_2$ [40d]	245.7	90.2	89.8	114.2	108.0
$[i\text{-}Bu_2AlP(SiMe_3)_2]_2$ [40c]	247.6	91.0	89.0	117.1	106.3
$[Me_2AlAs(SiMe_3)_2]_2$ [40e]	253.6	91.7	88.3	115.0	108.1
$[Et_2AlAs(SiMe_3)_2]_2$ [40f]	253.5	91.0	89.0	115.0	107.6
$[i\text{-}Bu_2AlAs(SiMe_3)_2]_2$ [40b,c]	255.0	92.2	87.8	118.8	105.6
$[Et_2AlSb(SiMe_3)_2]_2$ [39]	272.6	91.7	88.3	117.3	107.3
$[i\text{-}Bu_2AlSb(SiMe_3)_2]_2$ [37]	274.4	93.7	86.3	121.2	102.7

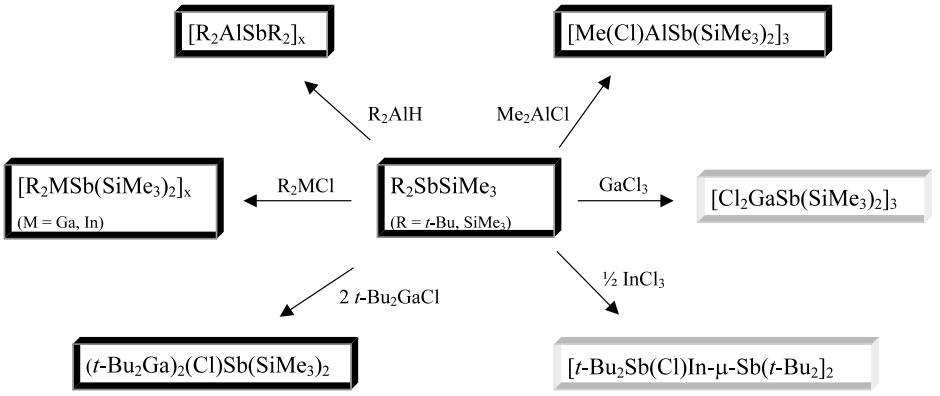

Scheme 2. Dehydro- and dehalosilylation reactions of $Sb(SiMe_3)$ and $t\text{-}Bu_2SbSiMe_3$.

3.2. Reactions

3.2.1. Exchange reactions

Both the four- and six-membered MSb heterocycles readily undergo exchange reactions with other Group 13/15 heterocycles in solution. This may occur through the breakage of one or two bonds within the ring, leading to the formation of chains or monomeric units of $R_2MER'_2$ in solution, which can rearrange to give the mixed ternary heterocycles.

$$[R_2MER_2]_2 + [R2ME'R_2]_2 \rightarrow (R_2M)_2(ER_2)(E'R_2) \quad (13)$$

$$[R_2MER_2]_2 + [R_2M'ER_2]_2 \rightarrow (R_2M)(R_2M')(ER_2)_2 \quad (14)$$

However, it is difficult to prove the existence of a ternary heterocycle unambiguously. NMR studies in solution always give complicated mixtures of compounds, and X-ray analysis is unable to distinguish between a 'real' ternary compound and a mixture (1:1 co-crystallization) of two different heterocycles. In addition, bond lengths and angles cannot be compared owing to disorder problems. The values observed are always 'mixed' values. This was found both in our group [42] and in Wells' group [33,43]. Therefore, the results of X-ray structure analyses will not be discussed herein. However, Wells and coworkers demonstrated the potential of so-prepared ternary compounds to produce ternary materials by thermal decomposition, as evidenced by XRD studies [33].

3.2.2. Ring cleavage reactions

Monomeric Group 13 monoamides, monophosphides and monoarsenides $R_2MER'_2$ (M = Al, Ga, In; E = N, P, As) have been synthesized and structurally characterized within the last 10 years. All of them are substituted by very bulky ligands (e.g. R, R′ = *t*-Bu, adamantyl, Mes* (2,4,6-*t*-Bu_3–C_6H_2), Dipp (2,6-*i*-Pr_3–C_6H_3), Cp*) to depress the tendency of cyclization or oligomerization. However, four- and six-membered heterocycles may be described as intermolecular stabilized Lewis acid–base adducts (Scheme 3).

As pointed out previously, the bond strength of Group 13 base adducts $R_3M \leftarrow D$ ($D = ER_3$) decrease from nitrogen to bismuth [7]. Corresponding to the HSAB

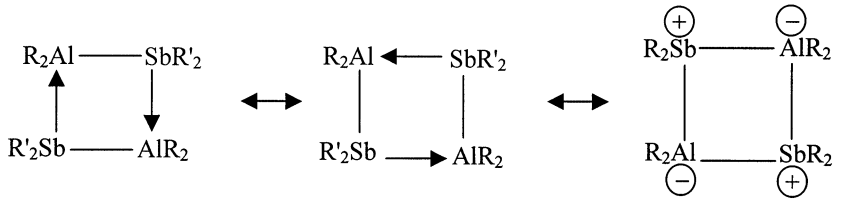

Scheme 3. Intermolecular stabilized heterocyclic acid-base adducts

concept, the 'hard' acid Al gives adducts with a 'hard' N-base rather than with 'soft' Sb- and Bi-bases. This tendency is also clearly demonstrated in reactions of equimolar amounts of the strong complexing N-base 4-dimethylamino pyridine (dmap) and the Al–Sb heterocycles $(R_2AlSb(SiMe_3)_2)_x$ (R = Me, $x = 3$ (**26**); R = Et (**28**), *i*-Bu, $x = 2$ (**29**)). For the first time, monomeric, Lewis base stabilized Al-monostibides $R_2AlSb(SiMe_3)_2 \leftarrow$dmap (R = Me (**31**), Et (**32**); Fig. 13) were formed after cleavage of the ring core [44].

$$1/x[R_2AlSb(SiMe3)_2]_x + \text{dmap} \rightarrow R_2AlSb(SiMe3)_2 \leftarrow \text{dmap} \quad (15)$$

Their solid state structures unambiguously prove the presence of monomeric units $R_2AlSb(SiMe_3)_2$, coordinated by one dmap molecule.

The Al–N distances (**31**: 1.978(1); **32**: 1.980(2) Å) are shorter than those observed in common Al–N adducts, which typically range from 2.00–2.10 Å [45]. The Al–Sb bond lengths (**31**: 2.691(1); **32**: 2.680(1) Å) are the shortest ever observed and are close to the sum of the covalent radii (264 pm). Therefore, we believe them to represent examples of 'real', undisturbed Al–Sb distances. Distances found within the AlSb heterocycles (2.72–2.78 Å) are significantly elongated (see Table 8). The environment around the Sb center is pyramidal (sum of the bond angles 302.4° (**31**) and 298.9° (**32**)). The Al atoms are tetrahedral arranged.

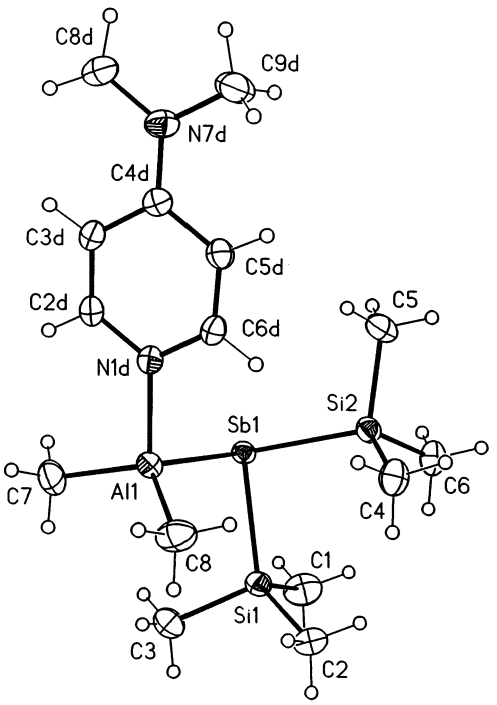

Fig. 13. Solid-state structure of **31**.

The reaction of heterocycles with dmap offers an elegant and general pathway for the synthesis of monomeric Group 13 stibides. These compounds are of interest owing to their potential to serve as starting compounds for the synthesis of bimetallic compounds of the type dmap → (R_2)Al–Sb(R'_2) → ML_n by coordination of a metal fragment ML_n to the Sb atom. Those compounds would show an interesting combination of a main group metal and a transition metal connected to one Group 15 element. Additionally, Lewis base stabilized monomers may be more volatile and, therefore, of greater interest in MOCVD processes than the heterocycles.

4. $[Me_2AlBi(SiMe_3)_2]_3$: synthesis and structure

The number of organometallic Bi-heterocycles $[R_xBiMR_x]_x$, containing Bi and the main group element M in 1:1 stoichiometry, is limited due to the weak M–Bi bonds (main group element). Almost every structurally characterized MBi heterocycle contains an electronegative element, like oxygen and nitrogen (M = O, N) [46]. $[Cp^*_2SmBi]_2$, containing a four-membered Sm_2Bi_2 core, is the only structurally characterized organometallic ring compound in which the Bi atoms are linked by an electropositive element [47].

We demonstrated the synthesis of an Al–Bi ring in excellent yields by dehydrosilylation. The reaction of Me_2AlH and $Bi(SiMe_3)_3$ gives $[Me_2AlBi(SiMe_3)_2]_3$ (**32**; Fig. 14), the first Group 13/15 compound with the heavier element of Group 15, Bi, which could be structurally characterized by single crystal X-ray analysis [48].

$$3Me_2AlH + 3Bi(SiMe_3)_3 \xrightarrow[-3Me_3SiH]{} [Me_2AlBi(SiMe_3)_2]_3 \ (\mathbf{33}) \quad (16)$$

As found in other six-membered heterocycles of the type $[R_2AlE(SiMe_3)_2]_3$ (E = P, As, Sb), the Al and Bi atoms of the non-planar six-membered ring adopt distorted tetrahedral environments. As expected, the endocyclic Al–Bi–Al bond angles (121.7(1)–130.5(1)°) are slightly bigger and the Bi–Al–Bi bond angles (101.0(1)–104.1(1)°) smaller than other Al-pnictogen rings due to the steric effects of the pnicogenides atom. Steric repulsion is responsible for the formation of either four- or six-membered heterocycles. With the smaller elements of Group 15, P and As (r_{cov}(P) = 110 pm; r_{cov}(As) = 119 pm), four-membered rings $[Me_2AlE(SiMe_3)_2]_2$ (E = P, As) are formed, whereas the somewhat larger Sb and Bi atoms (r_{cov}(Sb) = 138 pm; r_{cov}(Bi) = 146 pm) [26] favor the formation of six-membered rings $[Me_2AlE(SiMe_3)_2]_3$ (E = Sb, Bi) (Table 10).

The Al–Bi bond distances range from 275.5(3)–279.3(3) pm; this is longer than the sum of the covalent radii of 272 pm, but shorter than the distances found in the Zintl phase anion $[Al_2Bi_6]^{10-}$ in $Ca_5Al_2Bi_6$ (280.0–286.9 pm) [49]. Owing to the lack of other structurally characterized organometallic Group 13–Bi heterocycles, no further comparisons can be made.

The first synthesis of an organometallic Group 13–Bi compound clearly demonstrates the general application of the dehydrosylilation reaction to produce Group 13/15 compounds. Its major advantages are the mild reaction conditions (e.g. no

solvents are necessary; easy workup; quantitative yields; low reaction temperatures), which are necessary for the formation of this thermodynamically less stable Al–Bi ring, compared with other Al heterocycles with the lighter homologues of Group 15.

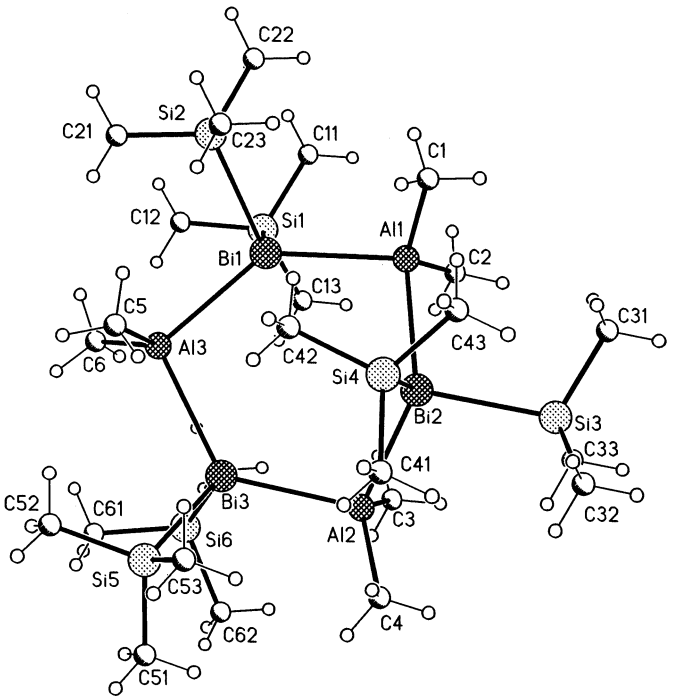

Fig. 14. Solid-state structure of **33**.

Table 10
Average bond distances and endocyclic bond angles of the six-membered heterocycles $[Me_2AlE(SiMe_3)_2]_3$ (E = P, As, Sb, Bi)

$[Me_2AlE(SiMe_3)_2]_x$	Al–E (pm)	Al–E–Al (°)	E–Al–E (°)	R–Al–R (°)	Si–E–Si (°)
E = P, $x = 2$[a] [35,72]	245.7	90.60	89.4	113.4	108.35
E = As; $x = 2$[a]	253.6	91.71	88.29	115.0	108.09
$[H_2AlP(SiMe_3)_2]_3$ [74]	239.8	126.42	113.58		107.83
E = Sb; $x = 3$ [23a]	271.9	124.01	104.89	117.88	101.65
E = Bi; $x = 3$ [46]	277.4	126.85	102.30	119.23	100.54

[a] The structures obtained for E = P and As show the presence of a four-membered ring $[Me_2AlE(SiMe_3)_2]_2$ in the solid state. Obviously, the Me group is sterically too demanding for the somewhat smaller P atom to allow the formation of a six-membered ring. However, the six-membered ring $[H_2AlP(SiMe_3)_2]_3$ is known and, therefore, is given in this table.

5. Binary, nanocrystalline MSb materials (M = Al, Ga, In)

Group 13 antimonides are narrow direct band gap semiconductors with small band gaps and high electron and hole mobilities, which render them very attractive for applications in optoelectronic devices (Table 11).

For example, GaSb is used for the production of light-emitting and light-detecting devices for the 2 μm wavelength range [50], in field effect transistors [51] and in infrared detectors [52].

Since the early 1990s, the preparation of *nanocrystalline* materials has been of industrial interest owing to their special electronic and optical properties [53]. Several synthetic routes, which lead to the formation of bulk materials, thin films and nanoparticles, have been explored. In Group 13/15 semiconductors, the preparation of phosphides and arsenides have been investigated extensively [54]. Recently, Wells and Gladfelter reviewed synthetic pathways for the preparation of binary and ternary nanocrystalline III–V (13–15) materials [54b]. Therefore, several studies described therein are not presented in this work. However, two pathways will be discussed here in more detail:

1. synthesis using chemical reactions in hydrocarbon solvents, and
2. pyrolysis of single-source precursors.

5.1. Synthesis in solution

In 1986, dehalosilylation reactions were established to prepare metalorganic Group 13/15 compounds [55] and in 1989, Group 13/15 materials were synthesized for the first time by this method [56]. Since that time, several groups have established this route to prepare ME materials (M = Al, Ga, In; E = P, As) of nanoscale dimension [57]. Group 13 antimonides had not been prepared until 5 years ago, when we [58] and Wells and coworkers [59] established the synthesis of GaSb by dehalosilylation reaction of $GaCl_3$ and $Sb(SiMe_3)_3$.

$$GaCl_3 + Sb(SiMe_3)_3 \xrightarrow[-3Me_3SiCl]{} \text{'GaSb'} \quad (17)$$

Detailed investigations on this reaction in different solvents at different temperatures clearly revealed the influence of the solvent on the GaSb nanoparticles formed [60]. Both the purity and the particle size of the so-formed GaSb depend on the solvent and its boiling point. We obtained the best results in xylene, achieving a uniform GaSb particle size, high homogeneity and low levels of impurities. Wells et al. also obtained good results from reactions in pentane [61]. Figs. 15 and 16 show typical transmission electron microscopy (TEM) images of GaSb samples prepared in xylene and hexane.

The different particle sizes obtained under almost the same reaction conditions (only the boiling point of the solvent differs) can clearly be recognized. With increasing temperature the particle size also increases, while the rate of impurity formation in the resulting material decreases. The hexane sample showed large particles with Moiré contrasts, indicating agglomeration of small stacked crystalline particles, which could be resolved by high-resolution TEM. The size of the single

Table 11
Band gaps and electron and hole mobilities at 300 K, melting points and emission wavelength of III–V materials [75]

Material	Energy gap (eV)	Electron mobility ($cm^2 V^{-1} s^{-1}$)	Hole mobility($cm^2 V^{-1} s^{-1}$)	Melting point (°C)	Emission λ (nm)
AlN	6.20		14	~2500	200
GaN	3.44	440		1500	380
InN	2.05	250		1200	620
AlP	3.62	60	450	~2100	500
GaP	2.27	160	135	1750	550
InP	1.34	5370–5900	150	1330	950
AlAs	2.15	75–294		2013	570
GaAs	1.42	8000–9200	400	1510	860
InAs	0.35	33 000	100–450	1215	3400
AlSb	1.61	200	400	1330	770
GaSb	0.75	3750	680	980	1800
InSb	0.17	77 000	850	798	7700

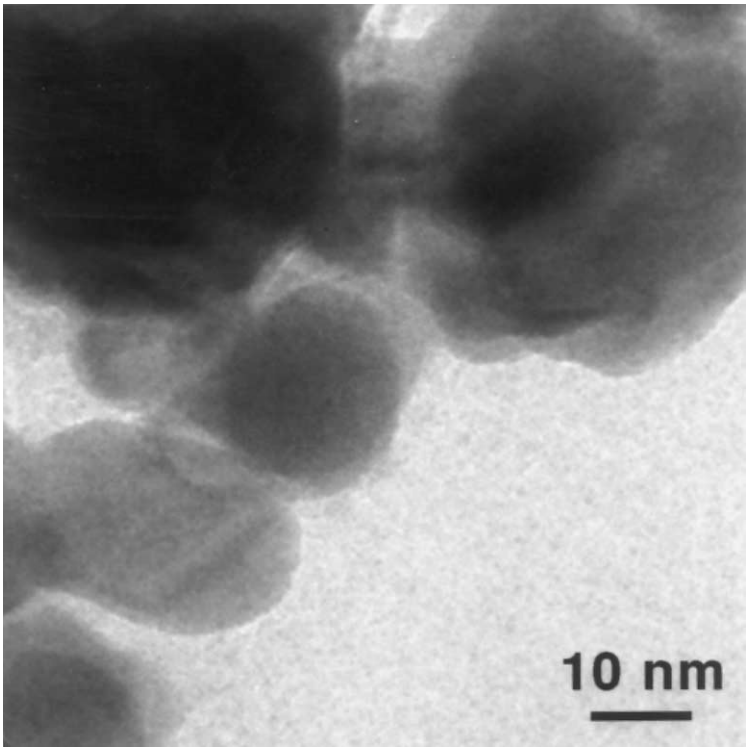

Fig. 15. TEM image of a GaSb sample prepared in hexane.

particles is about 10–15 nm with the lattice fringes having distances of 6 and 3.5 nm, belonging to (100) and (111) planes in cubic GaSb. The predominant GaSb particle size obtained from solution in xylene is about 50 nm. The XRD pattern of this sample compares well with reflections of cubic GaSb and some metallic Sb JCPDS [62]. The pattern of the xylene sample is also more crystalline, as indicated by sharper reflections and reduced background scattering. Rietveld refinement, based on the structure of sphalerite-type GaSb, leads to following lattice parameter of GaSb: $a = 609.52(2)$ pm (space group: $F\bar{4}3m$, Ga: 4*a* 0, 0, 0; Sb: 4*c* 1/4, 1/4, 1/4) ($R_{\text{prof}} = 5.83\%$, $R_{\text{Bragg}} = 1.22\%$).

This result is interesting, because the physical properties of semiconductors depend on their particle size [63]. Therefore, a simple, controlled synthesis of nanocrystals with a uniform particle size is the goal of several research activities.

5.2. Synthesis by pyrolysis of single-source precursors

5.2.1. Pyrolysis of $Sb(SiMe_3)_3$ adducts of gallium and indium trialkyls

The prepared adducts **6**–**17** (see Section 2) are potential precursors for CVD studies. The adducts sublime at relatively low temperatures (< 100°C at 10^{-3} mbar) without decomposition. First pyrolysis investigations at 350°C in sealed

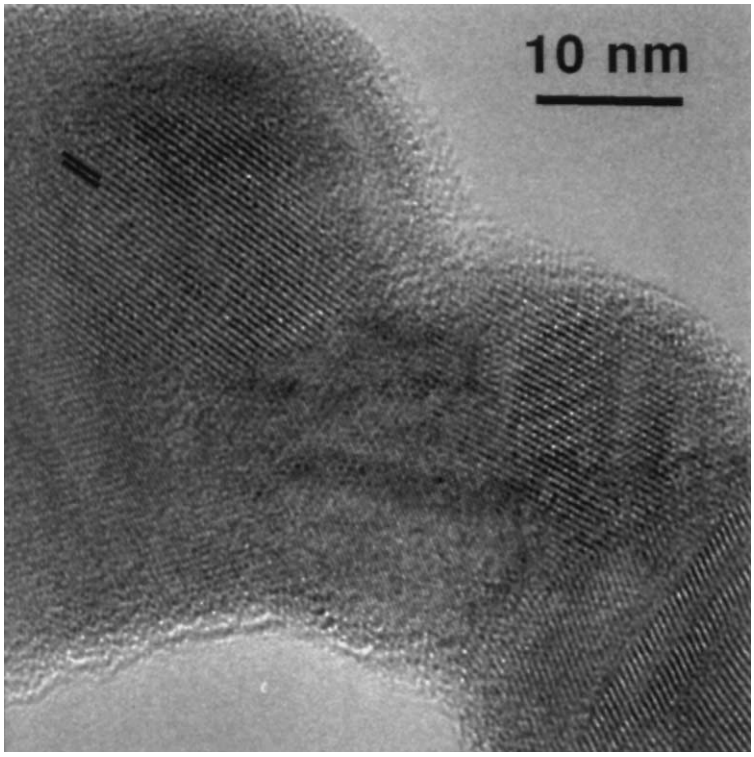

Fig. 16. TEM image of a GaSb sample prepared in xylene.

capillaries gave AlSb [64], GaSb and InSb [20] materials. Wells et al. studied the thermal decomposition of t-Bu_3Ga–$Sb(SiMe_3)_3$ (**14**) and t-Bu_3In–$Sb(SiMe_3)_3$ (**32**) under static vacuum at 350°C (**14**) and 400°C (**32**). Nanocrystalline GaSb and InSb, with an average particle size of 11 nm, were obtained through a β-hydride elimination pathway. Problems arose from the sublimation of the adducts under these conditions, leading to low final yields of 11% (**32**) and 30% (**14**). The thus-prepared InSb was In rich.

5.2.2. Thermal decomposition of GaSb and InSb heterocycles

The thermal decomposition behavior of $[t$-$Bu_2GaSb(SiMe_3)_2]_2$ **18** was investigated by two pyrolysis experiments [19b]:

1. pyrolysis between 175 and 400°C under *dynamic* vacuum resulted in the formation of GaSb in 64% yield with an approximate average particle size of 9 nm;
2. pyrolysis between 175 and 400°C under *static* vacuum resulted in the formation of GaSb in 27% yield. CH_4, H_2, Me_3SiH and isobutylene were eliminated and identified by IR spectroscopy, showing that the formation of the GaSb material occurs through a β-hydride elimination process.

$[Et_2GaSb(SiMe_3)_2]_2$ (**20**) was also investigated concerning its potential application as a precursor for the preparation of GaSb [33]. Thermolysis at 400°C leads to the formation of nanocrystalline GaSb (average particle size 10 nm) in low yield (20%) due to sublimation of the heterocycle under these conditions. The thus-formed GaSb shows contamination with C and H (2%). Again, its formation occurs through a β-hydride elimination.

Very recently, In-rich InSb was produced in 53% yield from the pyrolysis of $[t\text{-}Bu_2InSb(SiMe_3)_2]_2$ (**22**) at 400°C under static vacuum [20]. Interestingly, the material, also formed through a β-hydride elimination pathway, is free from contamination with carbon or hydrogen.

5.3. Synthesis of AlSb thin films by MOCVD process

Antimony-containing films have been grown by MOCVD, MBE [65] and metalorganic molecular beam epitaxy (MOMBE) [66], the combination of MOCVD and MBE. Problems for MOCVD preparations arise from the fact that potential precursor compounds are not stable at room temperature (e.g. SbH_3 decomposes at room temperature and Me_2SbH above -78°C). Moreover, primary and secondary stibines $RSbH_2$ and R_2SbH are difficult to generate and to handle. Therefore, MSb films (M = Al, Ga, In) were formed by reaction of Group 13 trialkyls, such as R_3M (R = Me, Et, *i*-Pr, *t*-Bu; M = Al, Ga, In) or $Me_3N \rightarrow AlH_3$, with Sb trialkyls, such as Me_3Sb, Et_3Sb and *t*-$BuSbMe_2$ [67]. Another Sb source for the preparation of Group 13 stibides by the MOCVD process is $Sb(NMe_2)_3$ [68]. However, various drawbacks from the use of two precursors, such as the site-blocking effect [62a], the formation of droplets on the surface of Group III elements [61c,63b], and a relatively low growth rate, have led to the search for alternative precursors.

Cowley et al. [10b] demonstrated the potential of the InSb heterocycle $[Me_2InSb(t\text{-}Bu)_2]_3$ (**3**) to produce polycrystalline InSb by MOCVD. InSb (stoichiometry In:Sb = 1:1) was grown on Si(100) wafers in a horizontal hot-wall reactor. The deposition temperature was 450°C and the growth rates $\sim 1.0\ \mu m\ h^{-1}$. The carbon impurity level was below the detection limit of X-ray photoelectron spectroscopy. Preliminary experiments also demonstrated $[Me_2GaSb(t\text{-}Bu)_2]_3$ (**2**) to be a useful precursor for the deposition of GaSb thin films. To the best of our knowledge, no further investigations concerning MOCVD preparations of Ga–Sb or In–Sb materials using heterocyclic single-source precursors were performed. The analogous preparation of AlSb thin films by this technology was also unknown, because, prior to our own results, no such AlSb heterocycles that could be used as starting compounds were known.

When designing a precursor for MOCVD experiments, the following aspects have to be considered.

1. The precursor has to be volatile enough to guarantee a sufficient mass transport.
2. The ring core has to be as stable as possible, while the metal–ligand bonds should be as weak as possible. It is known that the metal–carbon bond strength decreases with increasing size of the ligand [69], e.g. $GaMe_3$: $D^\circ_{298} = 264 \pm 17\ kJ\ mol^{-1}$; $GaEt_3$: $D^\circ_{298} = 209 \pm 17\ kJ\ mol^{-1}$; $SbMe_3$: $D^\circ_{298} = 255 \pm 17\ kJ\ mol^{-1}$; $SbEt_3$: $D^\circ_{298} = 243 \pm 17\ kJ\ mol^{-1}$) [70].

3. The metal centers should be substituted by a hydrogen atom or an alkyl group containing a β-H atom to allow a β-H elimination process, which is known to produce pure films with low carbon impurities.

Detailed pyrolysis studies were performed with $[Et_2AlSb(SiMe_3)_2]_2$ (**28**) and $[i\text{-}Bu_2AlSb(SiMe_3)_2]_2$ (**29**) in a cold-wall MOCVD reactor in the absence of any carrier gas and at relatively high vacuum conditions [71]. The AlSb films were grown on polycrystalline Al_2O_3 substrates [72]. The optimum deposition temperatures were determined to be in the ranges 375–425°C (**28**) and 425–475°C (**29**). In the optimized temperature ranges the films showed the expected 1:1 stoichiometry. The deposition rate is mainly kinetically limited and ranges from 5 to 9 μm h^{-1}. Table 12 shows the composition of the films as determined by wavelength-dispersive X-ray spectroscopy (WDS) analyses.

*5.3.1. AlSb film from $[Et_2AlSb(SiMe_3)_2]_2$ (**28**)*

X-ray diffraction studies on AlSb films grown at temperatures above 375°C show characteristic peaks of crystalline AlSb. The crystallinity increases proportionally to the temperature. However, the Si incorporation level also increases with the temperature, in particular at temperatures above 450°C. At 500°C, it reaches almost 15%. Carbon incorporation is below the detection limits of WDS and oxygen was less than 1 at.%. The concentration of Sb stays constant at around 47% with a concentration ratio of [Al]:[Sb] close to 1.0 up to a temperature of 450°C. At higher temperatures the [Al]:[Sb] concentration ratio rises (1.28 at 500°C) as the rate of the Sb deposition decreases in favor of Si deposition. Obviously, the metal–ligand bonds were cleanly cleaved at temperatures below 425°C, whereas at higher temperatures the fragmentation of the silyl groups occurs, which leads to silicon atoms being deposited in the layer.

The morphology of the AlSb thin films has been examined by scanning electron microscopy (SEM). The particle sizes range from 300 to 700 nm. Images of the films show both single crystals and agglomerated particles present in the layers. The analyses reveal small changes of the surface morphology in particle size depending on the temperature. An increase of the deposition temperature leads to smaller

Table 12
Composition of the AlSb thin films obtained from MOCVD reactions as determined by WDS analyses at different deposition temperatures

Precursor	Deposition temp. (°C)	Al (%)	Sb (%)	Si (%)	Ratio Al/Sb
28	350	48	47	3	1.02
28	425	49	47	3	1.04
28	450	47	43	8	1.09
28	500	46	36	15	1.28
29	400	49	47	3	1.04
29	450	50	47	4	1.06
29	500	49	42	8	1.16
29	550	46	27	28	1.71

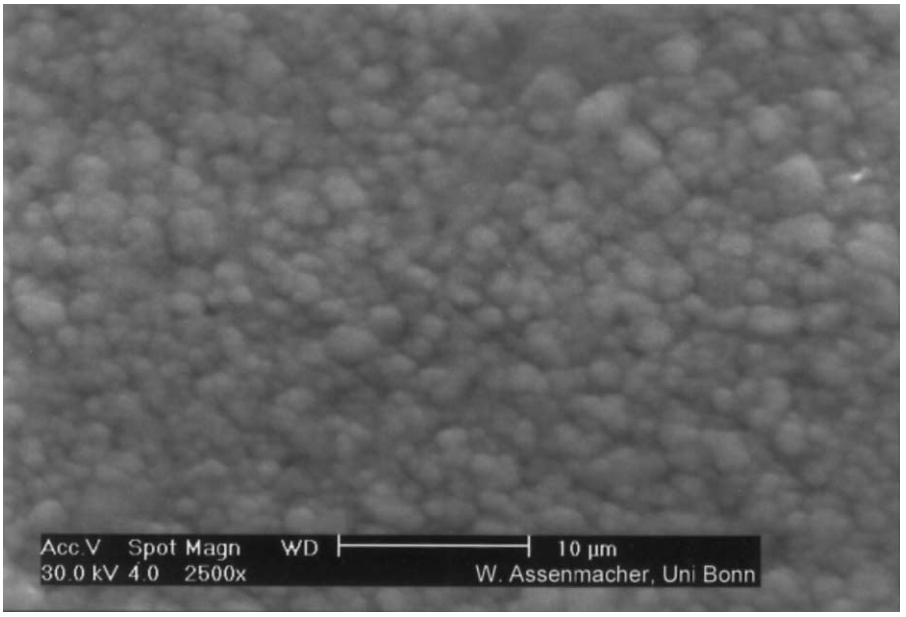

Fig. 17. AlSb thin film grown on Al_2O_3 at 425°C at a pressure of 5×10^{-5} mbar using precursor **28**.

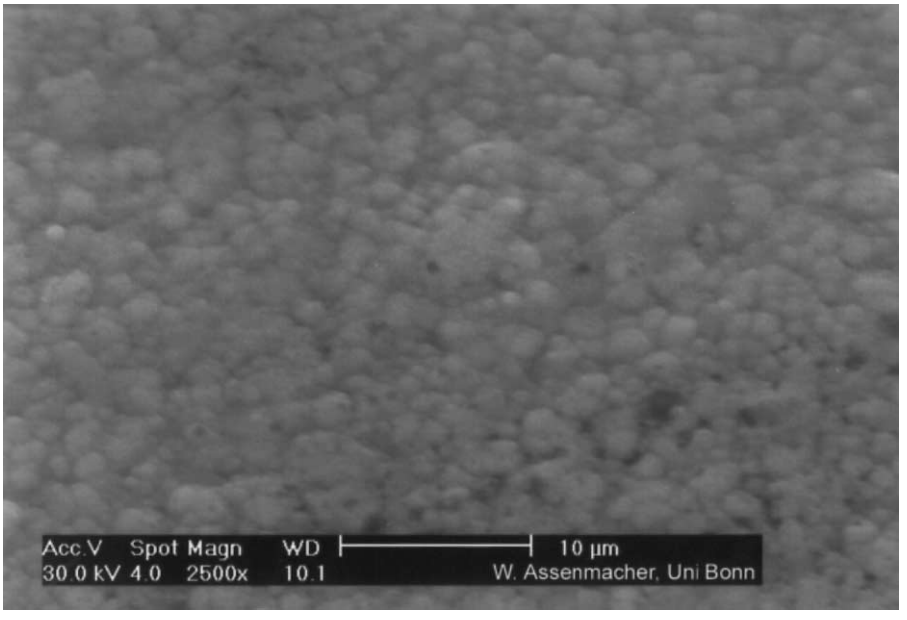

Fig. 18. AlSb thin film grown on Al_2O_3 at 475°C at a pressure of 5×10^{-5} mbar using precursor **29**.

crystallites. Figs. 17 and 18 show the results of the films grown on Al_2O_3 at 425°C and 475°C, respectively.

*5.3.2. AlSb film from [i-$Bu_2AlSb(SiMe_3)_2$]$_2$ (**29**)*

With precursor **29**, crystalline AlSb layers are formed above 425°C (about 50°C higher than with **28**). X-ray diffraction studies gave comparable results to films obtained from precursor **28**. Again, the composition of the films depends on the deposition temperature. At temperatures below 450°C the concentration of Si is low (3–4%). Above 475°C the Si concentration increases remarkably, reaching 27.5% at 550°C. The concentration ratio of [Al]:[Sb] is close to 1.0 at low temperatures. Above 475°C an Al-rich material is formed ([Al]:[Sb] = 1.7 at 550°C).

SEM studies of the films exhibit nearly the same surface morphology as those from precursor **28**. However, the particle sizes (in the range of 400–900 nm) are slightly larger.

6. Conclusions

Trialkyls of Group 13 R_3M react with SbR'_3 (R = alkyl, $SiMe_3$) to form simple Lewis acid–base adducts. In the solid state, the central M–E bond length is mainly a function of steric repulsion between the ligands. Sterically demanding Group 13 trialkyls, like *t*-Bu_3M, form the strongest adducts with electronically weaker, but sterically less bulky stibines. In contrast, Group 13 trialkyls with somewhat less bulky ligands, like Me and Et, form the strongest adducts with the electronically strongest stibines. Independent of their increased steric demand.

Ga–Sb and In–Sb heterocycles are formed by dehalosilylation reaction between dialkyl-gallium and -indium chlorides and $Sb(SiMe_3)_3$. The corresponding Al–Sb heterocycles can be obtained only by dehydrosilylation reactions using dialkyl aluminum hydrides and $Sb(SiMe_3)_3$ and $R'_2SbSiMe_3$, respectively. The ring size depends on the steric bulk of the substituents bound to Al.

The synthesis of $[Me_2AlBi(SiMe_3)_2]_3$ clearly demonstrates the general ability of the dehydrosilylation reaction for the synthesis of Group 13–pnicogenides compounds (pnicogenides = P, As, Sb, Bi). Al–Bi heterocycles, which are thermodynamically less stable than the corresponding compounds with the lighter elements of Group 15, can only be synthesized under those mild reaction conditions. No other reaction pathways succeeded.

In solution, the Group 13–Sb rings can be cleaved. This is evidenced by reactions of two different heterocycles, leading to mixed, ternary ring compounds. In addition, reactions of Al–Sb heterocycles with strong Lewis bases give monomeric, electronically stabilized Al–Sb compounds. This simple reaction offers the possibility to synthesize electronically rather than kinetically stabilized monomeric Group 13/15 compounds.

Binary Group 13–Sb materials can be produced by simple pyrolysis experiments of adducts or heterocycles by MOCVD reactions using the corresponding heterocycles and by reaction of $GaCl_3$ and $Sb(SiMe_3)_3$ in solution. Depending on the

hydrocarbon solvent, the composition, particle size and the crystallinity can be controlled.

Acknowledgements

I am very grateful to my co-worker A. Kuczkowski, who has prepared most of the completely alkylated Al–Sb compounds, and to Dr M. Nieger for the crystallographic work. I would also like to thank Professor H.W. Roesky, Universität Göttingen, and his co-worker, Dr H.S. Park, who performed the CVD studies with $[R_2AlSb(SiMe_3)_2]_2$ as well as (R = Et, *i*-Bu), as well as Professor W. Mader, Universität Bonn, and his co-worker, Dr W. Assenmacher, who studied the GaSb nanoparticles by energy-dispersive X-ray analysis and TEM. This work was supported financially by the DFG, the Fonds der Chemischen Industrie and the Bundesministerium für Bildung, Wissenschaft, Forschung und Technologie (BMBF), as well as by Professor E. Niecke, Universität Bonn.

References

[1] For example, see the following and references cited therein: (a) Y. Xie, R.S. Grev, J. Gu, H.F. Schaefer III, P.v.R. Schleyer, J. Su, X.-W. Li, G.H. Robinson, J. Am. Chem. Soc. 120 (1998) 3773. (b) F.A. Cotton, A.H. Cowley, X. Feng, J. Am. Chem. Soc. 120 (1998) 1795. (c) J. Müller, J. Am. Chem. Soc. 118 (1996) 6370. (d) W.H. Fink, P.P. Power, T.L. Allen, Inorg. Chem. 36 (1997) 1431. (e) T.L. Allen, A.C. Schreiner, H.F. Schaefer III, Inorg. Chem. 29 (1990) 1930.

[2] (a) Boron and Nitrogen. Gmelin Handbook of Inorganic and Organometallic Chemistry, 4th Supplement, Springer, Berlin, 1991 (Vol. 3a) and 1992 (Vol. 3b). (b) R.T. Paine, H. Nöth, Chem. Rev. 95 (1995) 343. (c) M.A. Petrie, M.M. Olmstead, H. Hope, R.A. Bartlett, P.P. Power, J. Am. Chem. Soc. 115 (1993) 3221. (d) M.A. Mardones, A.H. Cowley, L. Contreras, R.A. Jones, C.J. Carrano, J. Organomet. Chem. 455 (1993) C1. (e) G. Elter, M. Neuhaus, A. Meller, D. Schmidt-Bäse, J. Organomet. Chem. 381 (1990) 299. (f) P. Paetzold, Pure Appl. Chem. 63 (1991) 345. For a recent review see: (g) P.P. Power, Chem. Rev. 99 (1999) 3463.

[3] See for example: (a) K.M. Waggoner, H. Hope, P.P. Power, Angew. Chem. 100 (1988) 1765; Angew. Chem. Int. Ed. Engl. 27 (1988) 1699. (b) S. Schulz, L. Häming, R. Herbst-Irmer, H.W. Roesky, G.M. Sheldrick, Angew. Chem. 106 (1994) 1052; Angew. Chem. Int. Ed. Engl. 33 (1994) 969. (c) S. Schulz, A. Voigt, H.W. Roesky, L. Häming, R. Herbst-Irmer, Organometallics 15 (1996) 5252. (d) J.D. Fisher, P.J. Shapiro, G.P.A. Yap, A.L. Rheingold, Inorg. Chem. 35 (1996) 271. (e) R.J. Wehmschulte, P.P. Power, J. Am. Chem. Soc. 118 (1996) 791. (f) H. Hope, D.C. Pestana, P.P. Power, Angew. Chem. 103 (1991) 726; Angew. Chem. Int. Ed. Engl. 30 (1991) 691.

[4] H.M. Manasevit, Appl. Phys. Lett. 12 (1968) 156. Prior to this study, Didchenko et al. as well as Harrison and Tomkins described the synthesis of III–V material powders by reaction of Group 13 trialkyl and Group 15 hydrides. (a) R. Didchenko, J.D. Alix, R.H. Toeniskoettler, J. Inorg. Chem. 4 (1960) 35. (b) B. Harrison, E.H. Tomkins, Inorg. Chem. 1 (1962) 951.

[5] See for example: (a) A.H. Cowley, R.A. Jones, Angew. Chem. 101 (1989) 1235; Angew. Chem. Int. Ed. Engl. 28 (1989) 1208. (b) P.J. Brothers, P.P. Power, Adv. Organomet. Chem. 39 (1996) 1. (c) J.F. Janik, R.L. Wells, V.G. Young Jr, A.L. Rheingold, I.A.J. Guzei, J. Am. Chem. Soc. 120 (1998) 532. (d) R.L. Wells, R.A. Baldwin, P.S. White, W.T. Pennington, A.L. Rheingold, G.P.A. Yap, Organometallics 15 (1996) 91. (e) L.K. Krannich, C.L. Watkins, S.J. Schauer, C.H. Lake, Organometallics 15 (1996) 3980. (f) S.M. Stuczynski, R.L. Opila, P. Marsh, J.G. Brennan, M.L. Steigerwald, Chem. Mater. 3 (1991) 379.

[6] R.L. Wells, Coord. Chem. Rev. 112 (1992) 273.
[7] G.E. Coates, J. Chem. Soc. (1951) 2003.
[8] (a) L.K. Krannich, C.L. Watkins, D.K. Srivastava, Polyhedron 9 (1990) 289. (b) C.J. Thomas, L.K. Krannich, C.L. Watkins, Polyhedron 12 (1993) 89.
[9] S. Schulz, T. Schoop, H.W. Roesky, L. Häming, A. Steiner, R. Herbst-Irmer, Angew. Chem. 107 (1995) 1015; Angew. Chem. Int. Ed. Engl. 34 (1995) 919.
[10] (a) A.H. Cowley, R.A. Jones, K.B. Kidd, C.M. Nunn, D.L. Westmoreland, J. Organomet. Chem. 341 (1988) C1. (b) A.H. Cowley, R.A. Jones, C.M. Nunn, D.L. Westmoreland, Chem. Mater. 2 (1990) 221. (c) A.R. Barron, A.H. Cowley, R.A. Jones, C.M. Nunn, D.L. Westmoreland, Polyhedron 7 (1988) 77.
[11] For example, see the following and references cited therein: (a) A.R. Barron, J. Chem. Soc. Dalton Trans. (1988) 3047. (b) O.T. Beachley Jr, J.D. Maloney, Organometallics 16 (1997) 4016. (c) J.E. Park, B.-J. Bae, Y. Kim, J.T. Park, I.-H. Suh, Organometallics 18 (1999) 1059. (d) I. Krossing, H. Nöth, H. Schwenk-Kirchner, T. Seifert, C. Tacke, Eur. J. Inorg. Chem. (1998) 1925. (e) J. Müller, U. Ruschewitz, O. Indris, H. Hartwig, W. Stahl, J. Am. Chem. Soc. 121 (1999) 4647. (f) P.T. Brain, H.E. Brown, A.J. Downs, T.M. Greene, E. Johnsen, S. Parsons, D.W.H. Rankin, B.A. Smart, C.Y. Tang, J. Chem. Soc. Dalton Trans. (1998) 3685. (g) R.L. Wells, R.A. Baldwin, P.S. White, Organometallics 14 (1995) 2123. (h) R.L. Wells, A.T. McPhail, L.J.J. Jones III, M.F. Self, R.J. Butcher, Organometallics 11 (1992) 2694. (i) L.-J. Baker, L.A. Kloo, C.E.F. Rickard, M.J. Taylor, J. Organomet. Chem. 545 (1997) 249. (j) B. Beagley, S.M. Godfrey, K.J. Kelly, S. Kungwankunakorn, C.A. McAuliffe, R.G. Pritchard, J. Chem. Soc. Chem. Commun. (1996) 2179. (k) R.L. Wells, E.E. Foos, A.L. Rheingold, G.P.A. Yap, L.M. Liable-Sands, P.S. White, Organometallics 17 (1998) 2869.
[12] See for example: (a) A. Haaland, Angew. Chem. 101 (1989) 1017; Angew. Chem. Int. Ed. Engl. 28 (1989) 992. (b) A. Haaland, in: G.H. Robinson (Ed.), Coordination Chemistry of Aluminum, VCH, Weinheim, pp. 1–56.
[13] A.Y. Timoshkin, A.V. Suvorov, H.F. Bettinger, H.F. Schaefer, III, J. Am. Chem. Soc. 121 (1999) 5687.
[14] (a) R.G. Pearson, J. Am. Chem. Soc. 110 (1988) 7684. (b) W.B. Jensen, Chem. Rev. 78 (1978) 1.
[15] (a) C. Elschenbroich, A. Salzer, Organometallics, A Concise Introduction, second ed., VCH, Weinheim, 1992, pp. 84–87. (b) K.C.H. Lange, T.M. Klapötke, The Chemistry of Functional Groups: The Chemistry of Organic Arsenic, Antimony and Bismuth Compounds, Wiley, New York, 1994, p. 322. For the effect of d-contraction and lanthanoid contraction see p. 327.
[16] (a) M.G. Gardiner, C.L. Raston, Coord. Chem. Rev. 166 (1997) 1. (b) C. Jones, G.A. Koutsantonis, C.L. Raston, Polyhedron 12 (1993) 1829. (c) A.J. Downs, Coord. Chem. Rev. 189 (1999) 59.
[17] L.M. Nemirowskii, B.I. Kozyrkin, A.F. Lanstov, B.G. Gribov, I.M. Skvortsov, I.A. Sredinskaya, Dokl. Akad. Nauk SSSR 214 (1974) 590.
[18] M.S. Lube, R.L. Wells, P.S. White, J. Chem. Soc. Dalton Trans. (1997) 285.
[19] (a) R.A. Baldwin, E.E. Foos, R.L. Wells, P.S. White, A.L. Rheingold, G.P.A. Yap, Organometallics 15 (1996) 5035. (b) R.L. Wells, E.E. Foos, P.S. White, A.L. Rheingold, L.M. Liable-Sands, Organometallics 16 (1997) 4771.
[20] E.E. Foos, R.L. Wells, A.L. Rheingold, J. Cluster Sci. 10 (1999) 121.
[21] S. Schulz, M. Nieger, J. Organomet. Chem. 570 (1998) 275.
[22] S. Schulz, M. Nieger, J. Chem. Soc. Dalton Trans. (2000) 639.
[23] (a) S. Schulz, M. Nieger, Organometallics 18 (1999) 315. (b) S. Schulz, A. Kuczkowski, M. Nieger, J. Organomet. Chem. 604 (2000) 202.
[24] The structure of i-Bu_3Al–$Sb(SiMe_3)_3$ (**7**) was deposited as a private communication at the Cambridge Crystallographic Data Centre, CCDC No. 138649.
[25] M. Charton, Top. Current Chem. 114 (1982) 57.
[26] R.T. Sanderson, Chemical Bonds and Bond Energy, second ed., Academic Press, New York, 1976, p. 67. However, other textbooks give different values, e.g. $r_{cov}(Al) = 130$ pm, $r_{cov}(Ga) = 120$ pm. J. Huheey, E. Keiter, R. Keiter, Anorganische Chemie, Prinzipien von Struktur und Bindung, second ed., deGruyter, Berlin, 1995, p. 335.

[27] D.R. Lide, CRC Handbook of Chemistry and Physics, 78th ed., CRC Press, New York, 1997–1998, pp. 9-74.
[28] A. Leib, M.T. Emerson, J.P. Oliver, Inorg. Chem. 4 (1965) 1825.
[29] D.C. Bradley, H. Dawes, D.M. Frigo, M.B. Hursthouse, B. Hussian, J. Organomet. Chem. 325 (1987) 55.
[30] It is well known for phosphines R_3P that an increase of the substituent size leads to an increase of the basicity of the lone pair. The same is valid for stibines R_3Sb.
[31] Owing to the extreme sensitivity of the adducts in solution, molecular weight determination could not be performed. Therefore, we do not know the dissociation constants and dissociation enthalpies in solution.
[32] G.L. Wood, E.N. Duesler, C.K. Narula, R.T. Paine, H. Nöth, J. Chem. Soc. Chem. Commun. (1987) 496.
[33] E.E. Foos, R.J. Jouet, R.L. Wells, A.L. Rheingold, L.M. Liable-Sands, J. Organomet. Chem. 582 (1999) 45.
[34] H.J. Breunig, M. Stanciu, R. Rösler, E. Lork, Z. Anorg. Allg. Chem. 624 (1998) 1965.
[35] During the review process of this article Wells and coworkers published a paper containing the X-ray structure of $[Et_2InSb(SiMe_3)_2]_3$. E.E. Foos, R.J. Jouet, R.L. Wells, P.S. White, J. Organomet. Chem. 598 (2000) 182.
[36] The solid-state conformation could not be determined in detail owing to the disorder of the Cl and Me groups. However, the data set collected undoubtly confirms the presence of a six-membered ring [23a].
[37] S. Schulz, A. Kuczkowski, M. Nieger, Organometallics 19 (2000) 699.
[38] The following heterocycles show almost the same bond angles: $[Me_2AlAs(CH_2SiMe_3)Ph]_3$ (118.2(2)–122.2(2)° for Al–As–Al and 102.6(2)–104.8(2)° for As–Al–As); $[Me_2AlAsPh_2]_3{\cdot}(C_7H_8)_2$ (118.1(1)–122.7(1)° for Al–As–Al and 99.1(1)–101.1(1)° for As–Al–As); $[Me_2AlN(CH_2)_2]_3$ (119.9(5)° for Al–N–Al and 102.0(5)° for N–Al–N).
[39] S. Schulz, M. Nieger, Organometallics 17 (1998) 3398.
[40] (a) F. Hey-Hawkins, M.F. Lappert, J.L. Atwood, S.G. Bott, J. Chem. Soc. Dalton Trans. (1991) 939. (b) L.K. Krannich, C.L. Watkins, S.J. Schauer, Organometallics 14 (1995) 3094. (c) L.K. Krannich, C.L. Watkins, S.J. Schauer, C.H. Lake, Organometallics 15 (1996) 3980. (d) R.L. Wells, A.T. McPhail, M.F. Self, J.A. Laske, Organometallics 12 (1993) 3333. (e) R.L. Wells, A.T. McPhail, T.M. Speer, Eur. J. Solid State Inorg. Chem. 29 (1992) 63. (f) R.L. Wells, A.T. McPhail, T.M. Speer, Organometallics 11 (1992) 960.
[41] Different values are given in: J. Huheey, E. Keiter, R. Keiter, Anorganische Chemie, Prinzipien von Struktur und Bindung, second ed., deGruyter, Berlin, 1995, p. 335. The sum of the covalent radii are given as r_{cov}Al–Sb = 273 pm and r_{cov}Ga–Sb = 263 pm.
[42] Some mixed III–V compounds have been prepared and investigated structurally. In all cases four-membered heterocycles with disordered Al/Ga, As/Sb or P/Sb (50% occupancy) were obtained.
[43] (a) R.L. Wells, S.R. Aubuchon, M.S. Lube, P.S. White, Main Group Chem. 1 (1995) 221. (b) S.R. Aubuchon, M.S. Lube, R.L. Wells, Chem. Vap. Deposition 1 (1995) 28. (c) J.A. Laske-Cooke, R.L. Wells, S.R. Aubuchon, P.S. White, Organometallics 14 (1995) 3562. (d) L.J. Jones, A.T. McPhail, R.L. Wells, Organometallics 13 (1994) 2504.
[44] S. Schulz, M. Nieger, Organometallics 19 (2000) 2640. $H_3Al \leftarrow NMe_3$ reacts with sterically bulky secondary amines under the formation of Me_3N stabilized monomeric aminoalanes (a) J.L. Atwood, G.A. Koutsantonis, F.-C. Lee, C.L. Raston, J. Chem. Soc. Chem. Commun. (1994) 91. (b) M.G. Gardiner, G.A. Koutsantonis, S.M. Lawrence, F.-C. Lee, C.L. Raston, Chem. Ber. 129 (1996) 545. To the best of our knowledge, the only examples of Lewis base stabilized monomeric Group 13/15 compounds with the higher homologues of Group 15 were prepared by reaction of $H_3Al \leftarrow NMe_3$ with $As(SiMe_3)_3$ and $H_2AlCl \leftarrow NMe_3$ with $LiEMes_2$ (E = P, As), leading to the formation of $H_2AlAs(SiMe_3)_2 \leftarrow NMe_3$ (J.F. Janik, R.L. Wells, P.S. White, Inorg. Chem. 37 (1998) 3561) and $H_2AlPMes_2 \leftarrow NMe_3$ (D.A. Atwood, L. Contreras, A.H. Cowley, R.A. Jones, M.A. Mardones, Organometallics 12 (1993) 17). In addition, one example of a Lewis acid and Lewis base stabilized, monomeric compound, $Cr(CO)_5[Ph_2PAl(CH_2SiMe_3)_2 \leftarrow NMe_3]$ is known. (C. Tessier-Youngs, C. Bueno, O.T. Beachley Jr, M.R. Churchill, Inorg. Chem. 22 (1983) 1054). However, as far as we

know, no example of structurally characterized, monomeric, Lewis base stabilized Group 13/15 compounds obtained by a ring cleavage reaction has been described so far.

[45] A. Haaland defines a typical Al–N dative bond length to be 208 pm [12]. However, structurally characterized adducts display significant distance differences, e.g. Me_3Al–NMe_3 210(1) pm (G.A. Anderson, F.R. Forgaard, A. Haaland, Acta Chem. Scand. 26 (1972) 1947); H_3Al–NMe_3 206.3(8) pm (gas phase) (A. Almenningen, G. Gundersen, T. Haugen, A. Haaland, Acta Chem. Scand. 26 (1972) 3928); Me_3Al–NH_3 200.4(5) pm (powder diffraction) (J. Müller, U. Ruschewitz, O. Indris, H. Hartwig, W. Stahl, J. Am. Chem. Soc. 121 (1999) 4647); Cl_3Al–NMe_3 196(1) pm (D.F. Grant, R.C.G. Killean, J.L. Lawrence, Acta Crystallogr. Sect. B 25 (1969) 377); Cl_3Al–$NH_2(t\text{-Bu})$ 194 pm (W. Clegg, U. Klingebiel, J. Neemann, G.M Sheldrick, J. Organomet. Chem. 249 (1983) 47).

[46] For example, see the following and references cited therein: (a) C.M. Jones, M.D. Burkart, R.E. Bachman, D.L. Serra, S.-J. Hwu, K.H. Whitmire, Inorg. Chem. 32 (1993) 5136. (b) C.M. Jones, M.D. Burkart. K.H. Whitmire, Angew. Chem. 104 (1992) 466; Angew. Chem. Int. Ed. Engl. 31 (1992) 451. (c) U. Wirringa, H.W. Roesky, M. Noltemeyer, H.G. Schmidt, Inorg. Chem. 33 (1994) 4607.

[47] W.J. Evans, S.L. Gonzales, J.W. Ziller, J. Am. Chem. Soc. 113 (1991) 9880.

[48] S. Schulz, M. Nieger, Angew. Chem. 111 (1999) 1020; Angew. Chem. Int. Ed. Engl. 38 (1999) 967.

[49] G. Cordier, H. Schäfer, M. Stelter, Z. Naturforsch. Teil B 39 (1984) 727.

[50] A.Y. Polyakov, M. Stam, A.G. Milnes, R.G. Wilson, Z.Q. Fang, P. Rai-Choudhury, R.J. Hillard, J. Appl. Phys. 72 (1992) 1316.

[51] C.R. Bolognesi, E.J. Caine, H. Kroemer, IEEE Electron Device Lett. EDL-15 (1994) 16.

[52] (a) L. Samoska, B. Brar, H. Kroemer, Appl. Phys. Lett. 62 (1993) 2539. (b) Y. Zhang, N. Baruch, W.I. Wang, Appl. Phys. Lett. 63 (1993) 1068.

[53] For example, see the following and references cited therein: (a) H. Weller, Angew. Chem. 105 (1993) 42; Angew. Chem. Int. Ed. Engl. 32 (1993) 41. (b) H. Weller, Angew. Chem. 108 (1996) 1159; Angew. Chem. Int. Ed. Engl. 35 (1996) 1079. (c) J.R. Heath, J.J. Shiang, Chem. Soc. Rev. 27 (1998) 65.

[54] For example, see the following and references cited therein: (a) R.L. Wells, S.R. Aubuchon, S.S. Kher, M.S. Lube, P.S. White, Chem. Mater. 7 (1995) 793. (b) R.L. Wells, W.L. Gladfelter, J. Cluster Sci. 8 (1997) 217. (c) S. Gao, D. Cui, B. Huang, M. Jiang, Mater. Res. Bull. 33 (1998) 1023. (d) T. Douglas, K.H. Theopold, Inorg. Chem. 30 (1991) 596. (e) T.J. Trentler, S.C. Goel, K.M. Hickman, A.M. Viano, M.Y. Chiang, A.M. Beatty, P.C. Gibbons, W.E. Buhro, J. Am. Chem. Soc. 119 (1997) 2172. (f) J. Jiang, A.K. Schaper, R. Schäfer, T. Hihara, J.A. Becker, Adv. Mater. 9 (1997) 343. (g) Y.-D. Li, X.-F. Duan, Y.-T. Qian, L. Yang, M.-R. Ji, C.-W. Li, J. Am. Chem. Soc. 119 (1997) 7869. (h) Y. Xie, P. Yan, J. Lu, W. Wang, Y. Qian, Chem. Mater. 11 (1999) 2619.

[55] C.G. Pitt, A.P. Purdy, K.T. Higa, R.L. Wells, Organometallics 5 (1986) 1266.

[56] R.L. Wells, C.G. Pitt, A.T. McPhail, A.P. Purdy, S. Shafieezad, R.B. Hallock, Chem. Mater. 1 (1989) 4.

[57] (a) For example, see the following and references cited therein: (a) M.A. Olshavsky, A.N. Goldstein, A.P. Alivisatos, J. Am. Chem. Soc. 112 (1990) 9438. (b) L. Butler, G. Redmond, D. Fitzmaurice, J. Phys. Chem. 97 (1993) 10 750. (c) S.R. Aubuchon, A.T. McPhail, R.L. Wells, J.A. Giambra, J.R. Bowser, Chem. Mater. 6 (1994) 82. (d) J.F. Janik, R.L. Wells, P.S. White, Inorg. Chem. 37 (1998) 3561. (e) J.F. Janik, E.N. Duesler, W.F. McNamara, M. Westerhausen, R.T. Paine, Organometallics 8 (1989) 506. (f) A.H. Cowley, R.A. Jones, M.A. Mardones, J.L. Atwood, S.G. Bott, Angew. Chem. 102 (1990) 1504; Angew. Chem. Int. Ed. Engl. 29 (1990) 1409. (g) J.F. Janik, R.L. Wells, V.G. Young Jr, A.L. Rheingold, I.A. Guzei, J. Am. Chem. Soc. 120 (1998) 532. (h) T.J. Trentler, S.C. Goel, K.M. Hickman, A.M. Viano, M.Y. Chiang, A.M. Beatty, P.C. Gibbons, W.E. Buhro, J. Am. Chem. Soc. 119 (1997) 2172. (i) H. Uchida, T. Matsunaga, H. Yoneyama, T. Sakata, H. Mori, T. Sasaki, Chem. Mater. 5 (1993) 716. (j) Y.-D. Li, X.-F. Duan, Y.-T. Qian, L. Yang, M.-R. Ji, C.-W. Li, J. Am. Chem. Soc. 119 (1997) 7869.

[58] S. Schulz, L. Martinez, J.L. Ross, Adv. Mater. Optics Electron. 6 (1996) 185.

[59] R.A. Baldwin, E.E. Foos, R.L. Wells, Mater. Res. Bull. 32 (1997) 159.

[60] S. Schulz, W. Assenmacher, Mater. Res. Bull. 34 (2000) 2053.

[61] The workup conditions were slightly different from those we used. After filtration, Wells heated the black solid to 400°C for 24 h, whereas we heated up to 250°C for only 2 h, [59]
[62] Joint Commitee on Powder Diffraction Standards (JCPDS), File No. 7-215, GaSb and File 35-732, Sb.
[63] (a) M.V. Rama Krishna, R.A. Friesner, J. Chem. Phys. 95 (1991) 8309. (b) J.H. Fendler, F.C. Meldrum, Adv. Mater. 7 (1995) 607. (c) J.R. Heath, J.J. Shiang, Chem. Soc. Rev. 27 (1998) 65. (d) G. Schmid, M. Bäumle, M. Geerkens, I. Heim, C. Osemann, T. Sawitowski, Chem. Soc. Rev. 28 (1999) 179.
[64] The thus-formed AlSb was Sb rich and contaminated with up to 10% carbon and silicon. The crystallinity was low. MOCVD experiments may produce crystalline, binary AlSb materials with less contamination because this process works under different conditions, e.g. pyrolysis under dynamical vacuum or pyrolysis with use of a carrier gas. Detailed studies of these reactions are currently under investigation. S. Schulz, unpublished results.
[65] (a) H.K. Choi, G.W. Turner, Z.L. Liau, Appl. Phys. Lett. 65 (1994) 2251. (b) J. Schmitz, J. Wagner, F. Fuchs, N. Herres, P. Koidl, J.D. Ralston, J. Cryst. Growth 150 (1995) 858. (c) M. Yano, K. Yamamoto, T. Utatsu, M. Inoue, J. Vac. Sci. Technol. B 12 (1994) 1133. (d) T. Makimoto, B. Brar, H. Kroemer, J. Cryst. Growth 150 (1995) 883.
[66] (a) K. Yamamoto, H. Asahi, K. Hidaka, J. Satoh, S. Gonda, J. Cryst. Growth 179 (1997) 37. (b) H. Asahi, T. Kaneko, Y. Okuno, S. Gonda, Jpn. J. Appl. Phys. 32 (1993) 2786. (c) H. Asahi, T. Kaneko, Y. Okuno, Y. Itani, K. Asami, S. Gonda, J. Cryst. Growth 120 (1992) 252.
[67] (a) M. Leroux, A. Tromson-Carli, P. Gibart, C. Vérié, C. Bernard, M.C. Schouler, J. Cryst. Growth 48 (1980) 367.(b) D.S. Cao, Z.M. Fang, G.B. Stringfellow, J. Cryst. Growth 113 (1991) 441. (c) G.J. Bougnot, A.F. Foucaran, M. Marjan, D. Etienne, J. Bougnot, F.M.H. Dellannoy, F.M. Roumanille, J. Cryst. Growth 77 (1986) 400. (d) W.-K. Chen, J. Ou, W.-I. Lee, Jpn. J. Appl. Phys. 33 (1994) L402. (e) D.H. Jaw, D.S. Cao, G.B. Stringfellow, J. Appl. Phys. 69 (1991) 2552. (f) C.W. Wang, M.C. Finn, S. Salim, K.F. Jensen, A.C. Jones, Appl. Phys. Lett. 67 (1995) 1384. (g) C.W. Wang, K.F. Jensen, A.C. Jones, H.K. Choi, Appl. Phys. Lett. 68 (1996) 400. (h) R.M. Biefeld, A.A. Allerman, S.R. Kurtz, J. Cryst. Growth 174 (1997) 593. (i) V.C.H. Chen, G.B. Stringfellow, D.C. Gordon, D.W. Brown, B.A. Vaartstra, Appl. Phys. Lett. 61(2) (1992) 204.
[68] (a) J. Shin, A. Verma, G.B. Stringfellow, R.W. Gedridge, J. Cryst. Growth 143 (1994) 15. (b) S. Salim, C.K. Lim, K.F. Jensen, Chem. Mater. 7 (1995) 329. (c) J. Shin, A. Verma, G.B. Stringfellow, R.W. Gedridge, J. Cryst. Growth 151 (1995) 1.
[69] G.S. Tompa, in: W.S. Rees, Jr (Ed.), CVD of Nonmetals: Semiconducting Materials, VCH, Weinheim, 1996, p. 229.
[70] D.R. Lide, CRC Handbook of Chemistry and Physics, 78th ed., CRC Press, New York, 1997–1998, pp. 9-67.
[71] H.S. Park, S. Schulz, H. Wessels, H.W. Roesky, Chem. Vap. Deposition 5 (1999) 179.
[72] The AlSb films obtained on a Si substrate showed no improvement in composition, growth rates, morphology and crystallinity.
[73] D.R. Lide, CRC Handbook of Chemistry and Physics, 78th ed., CRC Press, New York, 1997–1998, pp. 9-51.
[74] J.F. Janik, R.L. Wells, P.S. White, Inorg. Chem. 37 (1998) 3561.
[75] (a) N.B. Hannay, Semiconductors, Reingold, New York, 1959. (b) O. Madelung, Semiconductors, Group IV Elements and III–V Compounds, Springer, Berlin, 1991. (c) A.C. Jones, C.R. Whitehouse, J.S. Roberts, Chem. Vap. Deposition 1 (1995) 65.